11-19-1997

Impedance spectroscopy of bilayer lipid membranes and TiO_2 based solar cells

Uwe Hermes
Portland State University

THESIS APPROVAL

The abstract and thesis of Uwe Hermes for the Master of Science in Physics were presented July 17, 1997, and accepted by the thesis committee and the department.

COMMITTEE APPROVALS:

[redacted]
Pavel Smejtek, Chair

[redacted]
Erik Bodegom

[redacted]
Carl Wamser
Representative of the Office of Graduate Studies

DEPARTMENT APPROVAL:

[redacted]
Erik Bodegom, Chair
Department of Physics

****

ACCEPTED FOR PORTLAND STATE UNIVERSITY BY THE LIBRARY

by [redacted] on Nov. 19, 1997

ABSTRACT

The abstract of the thesis of Uwe Hermes for the Master of Science in Physics presented July 17, 1997.

Title: Impedance spectroscopy of bilayer lipid membranes and TiO_2 based solar cells.

It has been proposed in the literature that a novel class of biosensors can be based on a bimolecular layer of lipids supported on one side by a metallic surface. In order to estimate the potential of this system for the design of membrane sensors, we have studied properties of a two-electrode system consisting of a teflon insulated metallic wire and a Ag/AgCl electrode, both immersed in KCl solution. The lipid bimolecular layer was formed on the metal surface of the cut teflon insulated wire. The electrical conductivity properties of such a device were studied in the frequency range 20 Hz - 1 MHz using the methods of impedance spectroscopy.

The admittance spectra were analyzed in terms of equivalent circuits. We have searched for the simplest equivalent circuit that can reproduce, with one set of parameters simultaneously, the frequency dependence of the conductance and the susceptance. It was shown that it is possible to assign the individual R and C elements and the Warburg-type impedance of the equivalent circuit to physical units

present in the device and the measuring circuit. The presence of the Warburg-type impedance was assigned to the roughness of the interface at which the charge transfer is taking place. The major finding is that the use of equivalent RC circuits to represent electrical properties of devices based on self-assembled lipid bilayers formed on cut insulated wires is inadequate.

Another system that was studied by means of impedance spectroscopy was a solar cell based on porphyrin-sensitized porous TiO_2 layer in contact with I_2/I_3^- redox pair. To construct an equivalent circuit of the solar cell we have measured admittance spectra of the cell with an increasing number of components comprising the solar cell. In this manner it was possible to arrive at an equivalent circuit that can reproduce the experimental admittance spectra of the cell and to associate the circuit elements with the major structures or regions of the solar cell. We have discovered changes of the admittance spectra on illumination of this cell and identified the elements of the equivalent circuit that change in the presence of light.

IMPEDANCE SPECTROSCOPY OF BILAYER LIPID MEMBRANES AND TiO_2 BASED SOLAR CELLS

By
UWE HERMES

A thesis submitted in partial fulfillment of the
requirements for the degree of

MASTER OF SCIENCE
in
PHYSICS

Portland State University
1997

Acknowledgments

I want to thank all the people who have supported, helped and guided me throughout my research. First of all I want to thank Dr. Pavel Smejtek for providing the project, his all of his help and for his continuous motivation to keep me going.

I am grateful to Suman Cherian who provided her equipment for the TiO_2 based solar cell experiment. Working with her was a great pleasure. I want to express my gratitude to Robert Word and Margie Fyfield for correcting the English grammar of my thesis. Special thanks go to Dr. Erik Bodegom and the Physics Department for making my stay possible. Also Dr. Bodegom's instant help and support was always highly appreciated. I had a good time with Dr. Smejtek's workgroup: Dr. Shanru Wang, Dr. Sophia Gilmiarova and Robert Word. Dr. Shanru Wang's help preparing the lipid solutions was essential in order for me to succesfully conduct experiments.

I could not imagine having completed my thesis yet, if it were not for Armin Rest, who helped me by way of his experience, his help with LaTeX, the programming language Delphi; and for providing his program-units for my use. I wish Armin and

his fiancee Marlene the very best in Seattle. Thanks to all the nice people here in the Physics Department for the fun and laughter in the Physics Computer Lab during my many working hours: Shawn, Lynn, Alex, Thomas, Luis and many others.

Last but not least I want to thank the exchange program between Oregon and Baden-Württemberg, the Fulbright program and my parents who made my stay here possible at all.

Contents

List of Tables

List of Figures

Chapter 1

Introduction

1.1 Biosensors

Sensors are generally used to detect phenomena and convert properties of the phenomena into appropriately scaled signals. Any change in the phenomena causes a subsequent change in the signal produced. Since the beginnings of science, people have used sensors to measure phenomena that may, in fact, be invisible. A simple thermometer converts temperature into a visible column, whose height is dependent on temperature.

Biosensors usually convert biological phenomena into electrical signals. Many different types of sensors can be used in biological applications. In biomedical applications these can include quantities such as muscle displacement, blood pressure,

core body temperature, blood flow, or cerebrospinal fluid pressure. Medical applications are reviewed in Bergveld [Ber96]. Sensors for electrical phenomena, usually known as electrodes, play a special role in diagnostic and therapeutic applications.

Chemical sensors are concerned with identification or detection of particular chemical compounds, measuring the concentration of various chemical species and monitoring chemical activities.

1.2 Electrodes

Electric conductivity in solutions is determined by ions as charge carriers. Biosensors as electrodes, interact with these ionic charge carriers to transduce ionic currents into electron currents in wires and electronic instrumentation [Neu95].At the interface between an electrode and an ionic solution redox (reduction-oxidation) reactions need to occur for charge to be transferred between the electrode and the solution. These reactions can be represented by the following equations:

$$A^{m-} \rightleftharpoons A + me^-$$

$$C \rightleftharpoons C^{n+} + ne^-$$

where n is the valence of a cation producing material C, and m is the valence of an anion material A. For most electrode systems, the cations in solution and the metal of the electrodes are the same, so the atoms C are oxidized when they give

Metal and Reaction	Half-cell Potential, V
$Al \rightarrow Al^{3+} + 3e^-$	-1.706
$Ni \rightarrow Ni^{2+} + 2e^-$	-0.230
$H_2 \rightarrow 2H^+ + 2e^-$	+0.000 (by definition)
$Ag + Cl^- \rightarrow AgCl + e^-$	+0.223
$Ag \rightarrow Ag^+ + e^-$	+0.799
$Au \rightarrow Au^+ + e^-$	+1.680

Table 1: The half-cell potentials for materials and reactions encountered in biomedical applications. Values are from Neumann [Neu95].

up electrons and go in solution as positively charged ions. These ions are reduced when the process occurs in the reverse direction. In the case of the anionic reaction, the directions for oxidation and reduction are reversed. For the best operation of the electrodes, these two reactions should be reversible, that is, it should be just as easy for them to occur in one direction as the other.

The interaction between a metal in contact with a solution of metal ions produces a local charge determined by the concentration of the ions in solution near the metal surface. Charge neutrality is not maintained in this region, causing the electrolyte surrounding the metal to be at different electrical potential from the rest of the solution. Thus, a potential difference known as the half-cell potential is established between the metal and the bulk of the electrolyte. It is found that different characteristic potentials occur for different materials. Some of these potentials are summarized in Table 1. [Neu95]

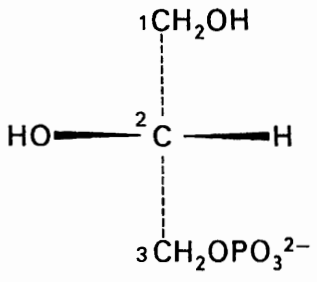

Figure 1: The absolute configuration of the glycerol 3-phosphate moiety of lipids (H and OH are in front of the page, whereas C-1 and C-3 are behind the page) [Str88].

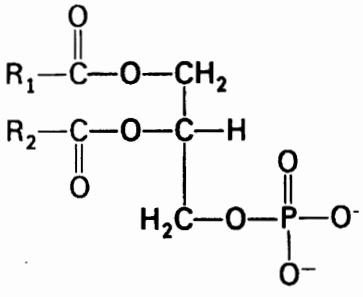

Figure 2: Phosphatidate(Diacylglycerol 3-phospate). R_1 and R_2 represent different hydrocarbon chains of fatty acids.

1.3 Lipids

Lipids are biomolecules that have high solubility in organic solvents such as chloroform and very low solubility in water. Lipids have a variety of biological roles: they serve as fuel molecules, as highly concentrated energy stores, and as components of membranes. Here, we are concerned with lipids as membrane constituents. There are three major kinds of lipids which are used to build membranes: phospholipids, glycolipids, and cholesterol.

Phospholipids are derived from either glycerol or sphingosine, which are both alcohols. A phosphoglyceride consists of a glycerol backbone, two fatty acid chains,

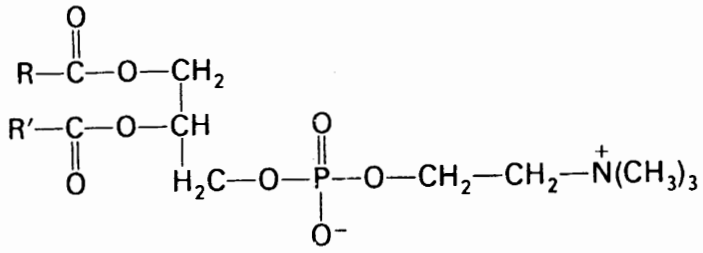

Figure 3: Structure model of a phosphatidylcholine molecule [Str88]. R and R' represent the hydrocarbon chains of fatty acids.

and a phosphorylated alcohol. The hydroxyl groups at C-1 and C-2 of glycerol (Figure 1) are esterified to the carboxyl groups of two fatty acid chains. The C-3 hydroxyl group is esterified to phosphoric acid. The resulting compound, called phosphatidate (or diacylglycerol-3-phosphate), is the simplest phosphoglyceride, Figure 2.

Fatty acid chains in phospholipids and glycolipids usually contain an even number of carbon atoms, typically between 14 and 24. The 16- and 18-carbon fatty acids are the most common ones. In animals and humans, the hydrocarbon chain of fatty acids is unbranched.

Fatty acids may be saturated or unsaturated, depending on the absence or presence of double bonds. The configuration of double bonds in unsaturated fatty acids is nearly always *cis*.

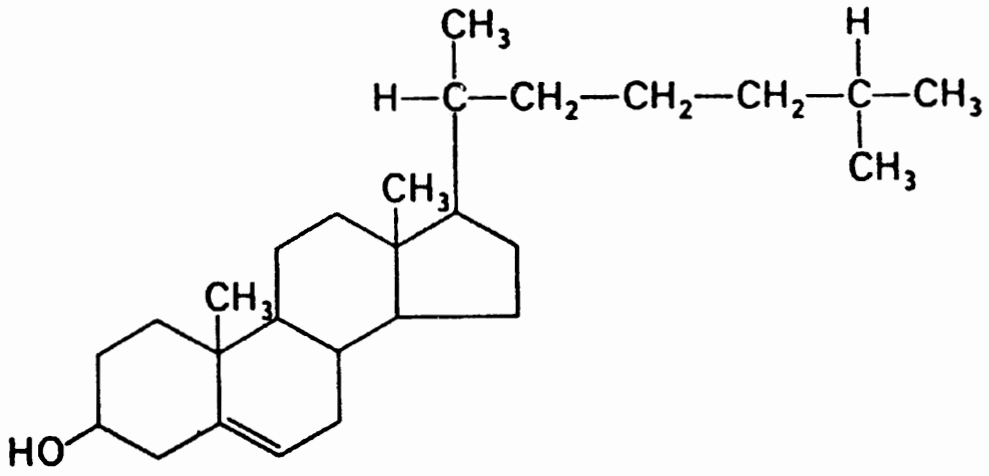

Figure 4: Structure model of the cholesterol molecule

The major phosphoglycerides are derivatives of phosphatidate. The phosphate group of phosphatidate becomes esterified to the hydroxyl group of one of several alcohols. The common alcohol moieties of phosphoglycerides are serine, ethanolamine, choline, glycerol, and inositol. [Str88]

To form a phosphatidyl choline (PC) a phosphatidate and a choline molecule must be attached to the phosphate group. The resulting structure formula can be seen in Figure 3. The other principal phosphoglycerides are phosphatidyl ethanolamine (PE), phosphatidyl serine (PS), phosphatidyl inositol, and diphosphatidyl glycerol.

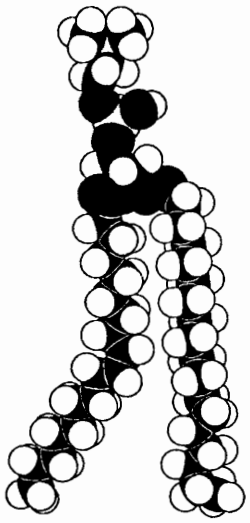

Figure 5: Space-filling model of the **phosphatidyl** choline molecule. Adapted from Stryer [Str88].

Glycolipids, as their name implies, are sugar-containing lipids. **Glycolipids,** like sphingomyelin, are derived from sphingosine. The amino group of the sphingosine is acylated by a fatty acid, as in sphingomyelin.

The third major lipid is cholesterol. It is present in eurocaryotes, but not in procaryotes or plants. Molecular structure is shown in Figure 4. Cholesterol is a steroid which alters membrane properties, for example its transition temperature.

1.4 Lipid Bilayers

The most critical common structural property of lipids is their amphipathic character, lipids contain both a hydrophilic and a hydrophobic moiety.

Consider, as an example, a space-filling model of a phosphoglyceride, such as PC shown in Figure 5. The two fatty acid chains are approximately parallel to one

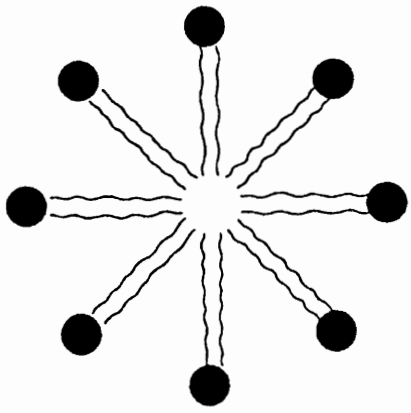

Figure 6: Diagram of a section of a micelle formed from phospholipid molecules

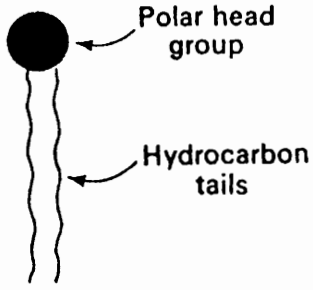

Figure 7: Symbol for a lipid molecule; the hydrophylic unit or polar head group represented by a circle, the hydrocarbon tails are depicted by waved lines

another, whereas the phosphatidyl choline moiety points in the opposite direction. All phosphoglycerides have similar geometry. The hydrophilic unit, also called the polar head group, is represented schematically by a circle, whereas their hydrocarbon tails are depicted by straight or waved lines, Figure 7

In aqueous medium several different aggregates of phosphoglycerides are possible:

Micelles: Micelles are spherical structures of lipids. The outer surface of these structures is made up of the polar head groups which participate in hydrogen

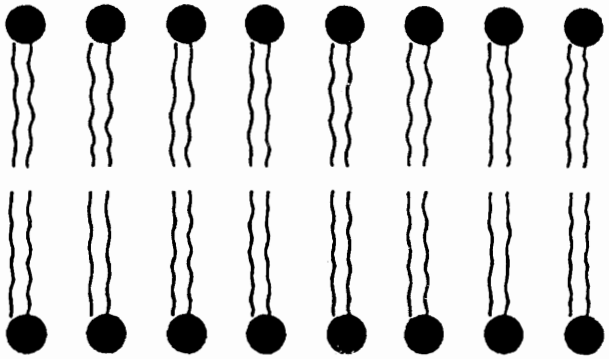

Figure 8: Diagram of a section of a bilayer membrane formed from phospholipid molecules

bonding with water. The inner part of the micelle is comprised of the hydrophobic tails. The final structure is shown in Figure 6 using the circle and wave lines representation for the phospholipids. The size of micelles is limited to about 200Å in diameter. [Str88]

Bilayer: Another arrangement that satisfies both the hydrophilic and hydrophobic preferences is a bimolecular sheet, also called a lipid bilayer. This is the most favored structure for most phospholipids and glycolipids in aqueous media. A model of a bilayer formed by phospholipids is shown in Figure 8. Because of the importance of the bilayer structure the space filling model of the bilayer is shown in Figure 9. Such a bimolecular sheet can have macroscopic dimensions up to 1-2 mm and is the matrix of all membranes.

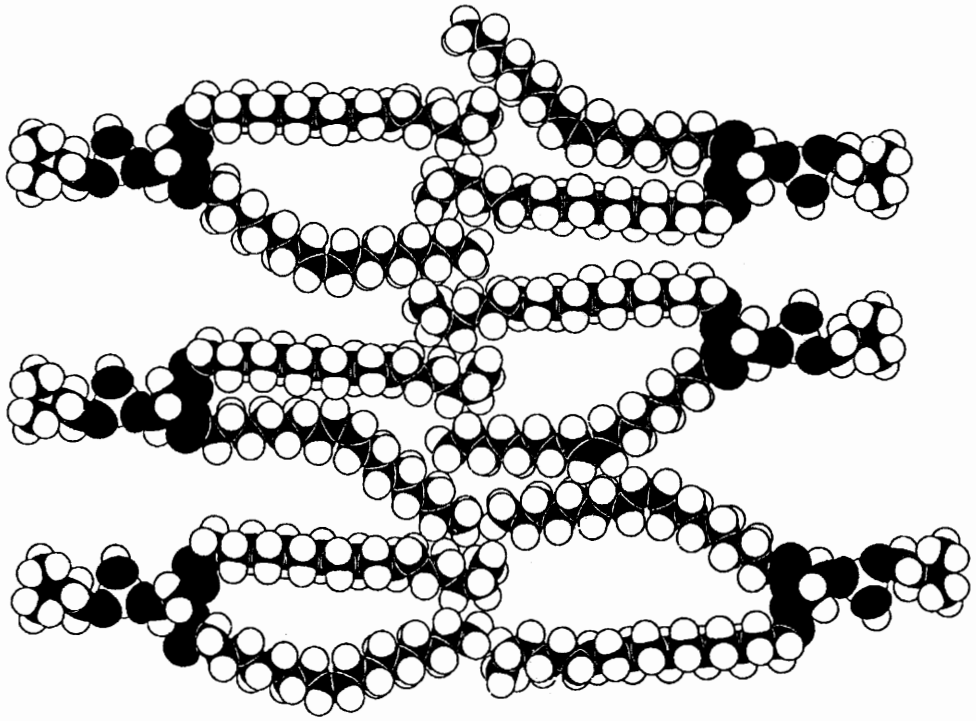

Figure 9: Space-filling model of a section of a bilayer. Because of the loose order this bilayer membrane is highly fluid.

Phospholipids and glycolipids are key membrane constituents of biological as well as artificial membranes because they readily form extensive bimolecular sheets. Furthermore, these sheets serve as a permeability barrier, even though the sheets are quite fluid. The formation of lipid bilayers is a self-assembly process. The formation of lipid bilayers from glycolipids and phospholipids is a rapid and spontaneous process in water. Hydrophobic interactions are the major driving force for the formation of lipid bilayers. [Str88]

One force contributing to the stability of lipid bilayers is the van der Waals attractive force between the hydrocarbon tails. This force maintains a close packing of the hydrophobic tails. In addition, there are favorable electrostatic and hydrogen-bonding interactions between the polar head groups and water molecules, that are also contributing to the stability of lipid bilayers.

Liposomes: Liposomes are aqueous compartments enclosed by a lipid bilayer. They are spherical or slightly elongated in shape and have a diameter of up to 1 - 2 micrometers. Liposomes can be formed by suspending a suitable lipid film in an aqueous medium. Liposomes prepared in this way are usually multi-lamellar. This mixture is then sonicated or extruded through submicron holes to yield a dispersion of liposomes that are quite uniform in size.

Drugs or DNA can be trapped in the aqueous compartment of liposomes. In this manner liposomes are used as drug and gene delivery in novel therapeutic applications.

1.5 Conventional self-assembled Bilayer Lipid Membranes

Bilayers have been established in science since the first report of self-assembled bilayer lipid membrane (BLM) in 1961 by Rudin, Tien and others on the Symposium

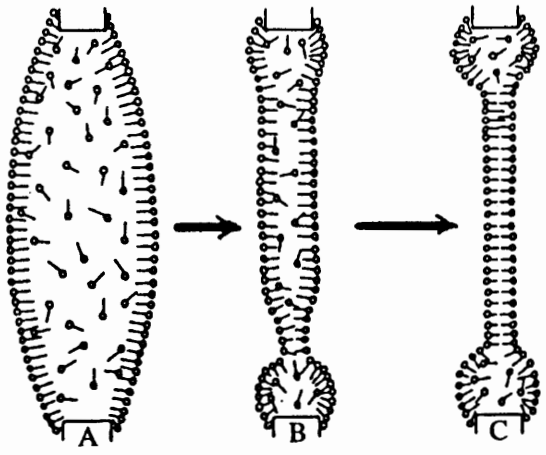

Figure 10: Thinning process of a conventional bilayer lipid membrane

on the Plasma Membrane. BLMs have been used and studied in a number of applications, ranging from basic membrane biophysical studies to the latest biosensor developments using supported bilayer lipid membranes.

Conventional or black lipid membranes were studied as a separator of two aqueous solutions. It is usually formed by spreading a lipid solution over a hole, which spontaneously thins to a BLM [Tie74]. (For example a drop of lipid solution, e.g. a 1% phospatidylcholine in n-decane may be spread over the hole. As the solvent drains away, a BLM is formed.) The thinning process is shown schematically in Figure 10. Formed in this fashion, changes in trans-BLM properties, such as electrical potential and current, can be readily measured by reference electrodes on either side of the membrane. To date this method is still one of the simplest techniques and widely used. [OT97]

A conventional BLM can also be formed by a modified Langmuir-Blodgett (LB) technique. This method essentially uses a lipid monolayer spread over the aqueous phase filling each side of a chamber separated by a vertical wall. The vertical wall contains a small hole above the solution. Raising the aqueous solution level on both sides above the hole results in the two monolayer combining into a BLM in the aparture.

The electrical properties of conventional BLMs are established [Tie74]:

- capacitance $C_m \simeq 0.3 - 1.3\ \mu\ \mathrm{Fcm}^{-2}$
- resistance $R_m \simeq 10^6 - 10^9\ \Omega\ \mathrm{cm}^2$
- dielectric breakdown $V_b \simeq 100 - 550\ \mathrm{mV}$

1.6 Supported self-assembled BLMs

The conventional BLM system has the disadvantage of instability. It is rarely stable more than several hours.

Bilayer lipid membranes formed on surfaces are found more stable. These supported BLMs (s-BLMs) can be formed on metallic wires, conducting SnO_2 glass, gel substrates and recently on microchips. Supported bilayer lipid membranes have been found to be stable over days and show a higher dielectric breakdown voltage. Some methods to build a supported BLM:

- BLMs can be formed on the tip of a metallic wire. The technique involves two steps: First, to place a teflon coated metal wire in a lipid solution and then to cut it using a sharp knife or miniature guillotine. Lipids adhere to clean freshly cut metal surface. The wire is then immersed into an aqueous solution for example KCl to form the bilayer.

- The formation of a gel supported BLM consists of three steps. In the first step, a chloridized Ag wire (Ag/AgCl) is inserted into Teflon tubing which has been previously filled with a solution of agar in KCl saturated with AgCl. The AgCl electrode and the filled Teflon tubing are then glued together. In the second step, the tip of the other end of this Teflon salt bridge is cut with a sharp knife again while immersed in a BLM-forming solution. The third step, the Ag/AgCl-Teflon salt bridge with the tip freshly coated with lipid solution is then immersed in the bathing solution, e.g. again KCl.

- A common technique is to prepare gold electrodes, for example on glass, as described in [S$^+$96]. A self-assembly monolayer of thiol-phospholipids is formed on the cleaned gold surface. On this first monolayer another monolayer is built to obtain a bilayer lipid membrane using different preparation methods. BLMs built in this way, were studied by means of impedance spectroscopy in terms

of simple RC circuits [S+96], [PGY94]. Examples of equivalent circuits are shown in Figure 13.

1.7 Supported BLMs as Biosensors

Attempts have been made to use supported BLMs as sensors in many different fields. A BLM supported on a metallic wire performed as a detector for the presence of potassium ferri/ferrocyanide and hydrogen peroxide [OT97].

It was also found [OL+94] that modified supported BLMs can be used as pH sensors. Conventional glass electrodes as pH-meters are limited by its size whereas BLMs can be built in microstructures and opens the field to application of micro-electronic technologies

Another application of self-assembled supported BLMs are specific ion sensors. Experiments show that modified s-BLMs are sensitive to K^+ in the range of 10^{-4} to 10^{-1} M showing a Nernstian slope of 55 mV. Similar results are obtained for NH_4^+, Na^+ and Li^+ [OT97].

s-BLMs on Interdigitated Structures (IDS) (see Figure 11) enables a wide field for novel applications. Those BLM modified chips are obtained by forming s-BLMs on IDS made on platinum with a window of 0.5mm x 0.5mm. s-BLMs on an IDS can be manufactured using microelectronic technologies. Using bilayer lipid membranes

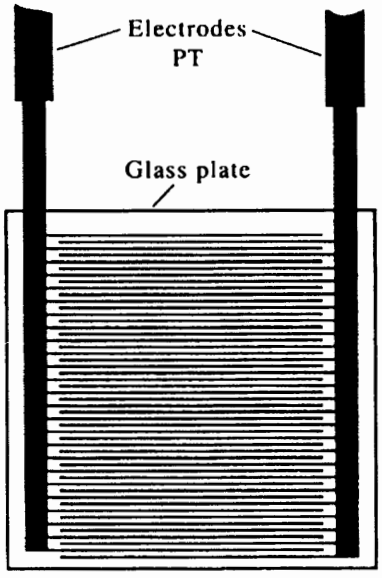

Figure 11: Interdigitated electrode array (IDS) adapted from Ottova and Tvarozek [OT97].

containing membrane receptors potentially open a host of physiological applications, such as ion/molecular recognition.

1.8 Colloidal TiO_2-films as solar-cells

Conventional solar cells are built either from single crystal or amorphous silicon. These cells have conversion efficiencies up to 18%. The energy cost to produce these cells is still very high, which limits their economic viability.

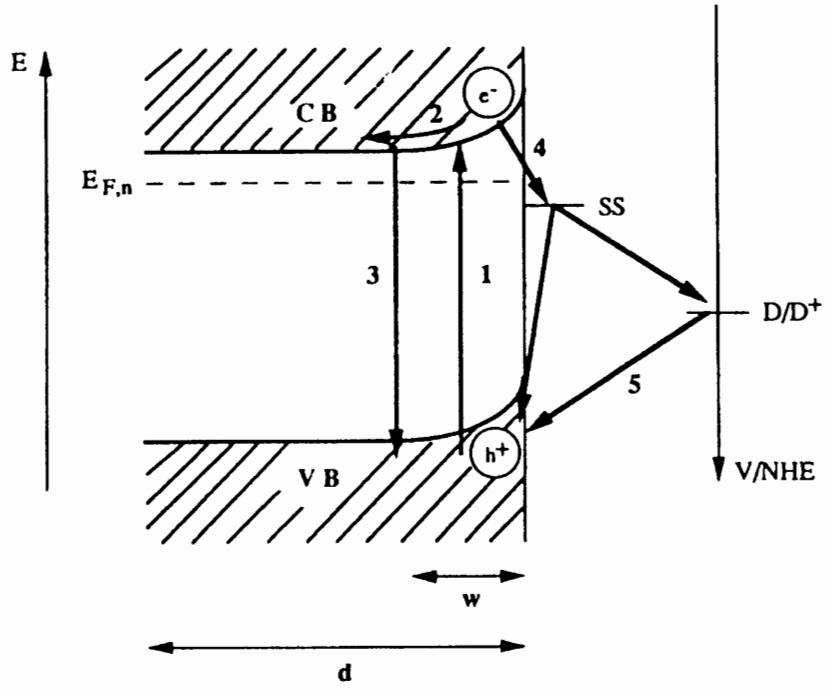

Figure 12: Energy-level diagram for a photoelectrochemical cell with zero external bias. The potential of a redox couple as well as the energy level of some surface state are indicated. The electrode thickness is d, the depletion layer width is indicated by w. Adapted from Hagfeldt [H⁺92].

Another approach for building solar cells is to use large gap semiconductors which are sensitized with dyes. An extraordinary high efficiency was found for colloidal TiO_2, which has a band gap of 3.2 eV.

Of crucial importance for a high efficiency of the solar cell is the charge process and the recombination processes at the semiconductor/electrolyte interface. The current model illustrating the energy levels at a semiconductor/electrolyte interface is depicted in Figure 12.

The conduction and the valence bands bend upwards at the band edge position. Figure 12 also indicates the Fermi level of a redox couple, on the electrochemical potential scale, and the energy level of a possible surface state. The different pathways that an excited electron can follow are also illustrated. Illumination of the semiconductor with light of energy exceeding the band gap, excites an electron from the valence band into the conduction band(1). In the depletion layer the electron is is drawn off as a photocurrent(2). Reactions limiting the photocurrent are electron-hole recombination in the band gap (3) and/or recombination via surface states (4) or via species in the electrolyte (5). For effective charge separation it is important how rapidly the positive vacancy in the valance band can be filled with an electron from the electrolyte. Rate limiting for this reaction can be the charge transfer process and/or the transport of the redox couple to and from the surface. If these processes are fast, recombination reactions will be less probable resulting in higher quantum efficiencies [H$^+$92].

Chapter 2

Impedance Spectroscopy

Life, electricity, and the relations between them have long been subjects of intense curiosity. After the Egyptian records of electric catfish about 2000 B.C., electrical phenomena in living things were brought into focus in 1790 by Galvani. The studies of conduction started as a description of living tissues as electrical conductors, and culminated in the formulation of Ohm's law in 1827 [Col68].

Electrochemical impedance spectroscopy (EIS) is now well established as a technique for investigating electrochemical and metal corrosion systems. The power of EIS lies in the fact that it is essentially a steady-state technique capable of measuring relaxation phenomena whose relaxation times vary over many orders of magnitude. The steady state character permits the use of signal averaging within a single experiment to gain the desired level of precision, and the wide frequency band width.

These features generally surpass the equivalent performance characteristics for the time domain experimental techniques. EIS has become one of the principal methods for investigating interfacial reaction mechanisms.[Mac90a]

2.1 Principles of Alternating-Current Electrodynamics

First we define the relationship between electrical current and applied voltage in cases of ohmic resistor, the capacitor, and the self-inductance. These elements are used to construct equivalent circuits of electrodes, membranes and solar cells.

1. If the alternating voltage is given by

   $$V = V_m \sin \omega t$$

   then the resulting current through a resistance R follows Ohm's law:

   $$i = \frac{V_m}{R} \sin \omega t$$

2. The current passing through a cicuit containing a condenser with capacitance C is determined by the relation between V and the charge q on the plates:

   $$q = CV$$

   $$i = \frac{dq}{dt} = C\frac{dV}{dt} = \omega C V_m \cos \omega t = \omega C V_m \sin(\omega t + \frac{\pi}{2})$$

3. The self-inductance L of a coil is defined such that

$$V = L\frac{di}{dt}$$

$$i = \frac{1}{L}\int V dt = -\frac{V_m}{\omega L}\cos\omega t = \frac{V_m}{\omega L}\sin(\omega t - \frac{\pi}{2})$$

In all three cases both i and V are sinusoidal functions of time. This means that the current-voltage relation can also be found starting with

$$i = i_m \sin\omega t'$$

and calculating the voltage across

1. a resistance

$$V = i_m R \sin\omega t'$$

2. a capacitance

$$V = \frac{q}{C} = \frac{1}{C}\int i dt = \frac{1}{\omega C}\sin(\omega t' - \frac{\pi}{2})$$

3. a self-inductance

$$V = L\frac{di}{dt} = \omega L \sin(\omega t' + \frac{\pi}{2})$$

Note that t and t' represent the time elapsed since respectively V and i passed through zero in the positive direction. The similar time dependence of current and voltage distinguishes sine wave signals from other time-dependent signals.

In general, an electric circuit consists of a number of conducting elements connected in series or in parallel. The behavior of such circuits is described by Kirchhoff's laws.

Evidently the relation between sine wave current and voltage is entirely descibed by two quantities, namely, the ratio of the amplitudes, $\frac{V_m}{i_m}$, and the phase shift ψ between current and voltage. [SRS70]

We can therefore define a two dimensional phasor Z, called the impedance, with modulus $|Z| = \frac{V_m}{i_m}$ and argument (phase angle) ψ. The impedance phasor is also defined by its components,

$$Z' = |Z|\cos\psi \qquad Z'' = |Z|\sin\psi$$

Now if $i = i_m \sin\omega t$, then for a certain impedance Z

$$\begin{aligned} V &= V_m \sin(\omega t - \psi) = i_m|Z|(\sin\omega t\cos\psi - \cos\omega t\sin\psi) \\ &= i_m(Z'\sin\omega t - Z''\cos\omega t) \end{aligned}$$

For several impedances in series we obtain

$$V = i_m(\Sigma Z'\sin\omega t - \Sigma Z''\cos\omega t)$$

conductor	Z'	Z''	Y'	Y''
resistance R	R	0	$\frac{1}{R}$	0
capacitance C	0	$\frac{1}{\omega C}$	0	ωC
self-inductance L	0	$-\omega L$	0	$-\frac{1}{\omega L}$

Table 2: The impedances and admittances of different conductors

For a parallel connection of circuit elements it is convenient to define the admittance Y as a phasor $|Y| = \frac{i_m}{V_m} = \frac{1}{|Z|}$ and argument ψ. Therefore,

$$Y' = |Y|\cos\psi \qquad Y'' = |Y|\sin\psi$$

For circuit elements in parallel, if $V = V_m \sin\omega t$

$$i = V_m(\Sigma Y' \sin\omega t + \Sigma Y'' \cos\omega t)$$

The impedances and admittances of the conductors mentioned above are summarized in Table 2.

2.2 Equivalent Circuits

For the interpretation of impedance spectra, equivalent circuit models are widely used. The equivalent circuit models also provide the opportunity to attribute physical meaning to the circuit parameters and to the circuit configuration used. It is often convenient to represent the real electrical and electrochemical properties of materials and interfaces with idealized equivalent electrical circuit models consisting of discrete electrical components.

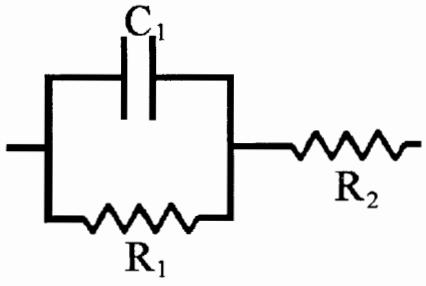

Figure 13: Circuit used to describe the interface of a thin layer on an electrode, R_2 representing the solution resistance, C_1 the layer capacitance depending on the thickness and R_1 representing conductivity through the layer.

Having found an appropriate equivalent circuit for a system, it is interesting to look at changes in the circuit parameters when other experimental parameters of the setup, or experimental conditions are changed in a systematic way.

The most often used equivalent circuit for electrode interfaces and thin layers is the circuit shown in Figure 13. Resistor R_2 represents the solution resistance in series with resistor R_1 representing the film resistance and capacitor C_1 representing the interface between the solution and the electrode.

2.3 Warburg Impedance

Warburg impedance has been introduced as a part of the faradaic impedance to account for diffusion processes. Starting with an "absolute rate equation" it was shown [SRS70], [War99] that the resulting impedance for the system is given by

$$Z'_\sigma = -Z''_\sigma = \sigma\omega^{-\frac{1}{2}} \tag{1}$$

$$Y'_\sigma = Y''_\sigma = \sigma^{-1}\omega^{\frac{1}{2}} \tag{2}$$

σ is given by $\sigma_O + \sigma_R$, where

$$\sigma_O = \frac{RT}{n^2F^2\sqrt{2}} \frac{D_O^{-1/2} exp(-\beta\phi)}{\alpha\bar{C}_R exp(\alpha\phi) + \beta\bar{C}_O exp(-\beta\phi)}$$

$$\sigma_R = \frac{RT}{n^2F^2\sqrt{2}} \frac{D_R^{-1/2} exp(-\beta\phi)}{\alpha\bar{C}_R exp(\alpha\phi) + \beta\bar{C}_O exp(-\beta\phi)}$$

with

$\bar{C}_R, \bar{C}_O$	"dc components" of the concentrations at the electrode surface, controlled by the mass transfer involved in the dc-process
D_R, D_O	diffusion constants for anodic and cathodic material
α, β	anodic and cathodic transfer coefficients; $\alpha + \beta = 1$
ϕ	eV/kT
V	applied voltage
n	charge multiplicity (valency) of charge carrier
R	universal gas constant $8.314 JK^{-1}mol^{-1}$
T	temperature
F	Faraday constant $96487 Cmol^{-1}$
e	charge of an electron $1.60210^{-19}C$
k	Boltzmann constant $1.3810^{-23}JK^{-1}$

The above equation define the originally introduced Warburg Impedance [War99]. A more general approach developed by Macdonald, called the finite-length Warburg

impedance, contains the original Warburg impedance, also referred as infinite Warburg impedance, as a limiting case. The general Warburg impedance can be written as

$$Z_W = R_{D0}[\tanh(\sqrt{is})/\sqrt{is}],$$

where $s = l_e^2(\omega/D)$, D is the diffusion coefficient and l_e the length of a finite region. [Mac87] [Mac90a]. For $l_e \to \infty, Z_W \to Z_\sigma$ with $\sigma = \frac{R_{D0}\sqrt{D}}{l_e\sqrt{2}}$.

Z_σ is a circuit element introducing a phase shift of $\theta = 45°$ in the complex plane. Experimentalists often introduce a constant phase element (CPE) into equivalent circuit, but without physical explanation. [Mac87]

2.4 Access Resistance

The access resistance of a circular pore is an important quantity for estimating the conductance of possible pores in biological membranes.

It can be shown that problems of resistance between electrodes in conducting media and problems of capacitance between electrodes in insulating media are related by a simple transformation [Smy50]. For a given electrode geometry, resistance and capacitance are related by the equation

$$R = \frac{\epsilon\rho}{C},$$

where R is the resistance, C the capacitance, ϵ the permitivity of the medium where the capacitance is measure, and ρ the resistivity of the medium where the resistance is measured.

The capacitance of a charged conducting disk is well known to be

$$C = 8\epsilon a,$$

where a is the radius of the disk.

The field and equipotential lines of this problem have exactly the same shape in either half-plane. It is only necessary to realize that our problem involves only one half space. Consequently the appropriate value of the capacitance is half the above value [Hal75]. The access resistor of the pore is thus

$$R_{conv} = \frac{\rho}{4a} \tag{3}$$

2.5 Graphical Presentation of Impedance

There are different ways to present the complex impedance graphically. A "Cole-Cole" plot is a well known presentation of experimental results in which the real part of the measured complex permittivity is plotted vs. the imaginary part. Such a complex permittivity plot can have any form. In their complex permittivity plots

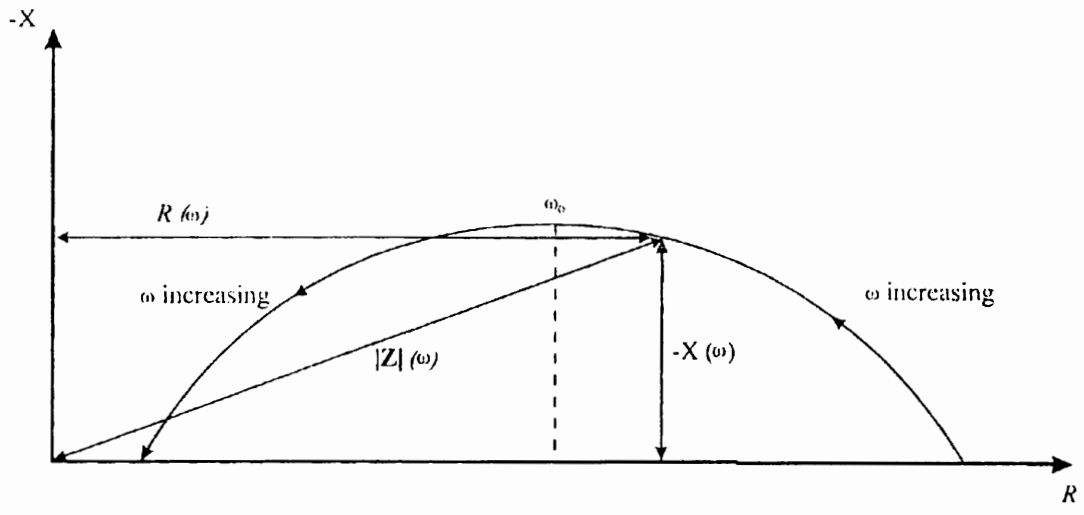

Figure 14: Cole-Cole plot showing a Single Impedance Arc

for a wide range of samples, Cole and Cole obtained semicircular arcs whose centers lay below the real axis similar to that shown in the complex impedance plane (Figure 14).

A plot of complex numbers using real and imaginary axes is termed an Argand diagram, a term sometimes used to describe the complex impedance plot shown in Fig. 14. A frequency-dependent impedance is better presented on a Nyquist plot. A modified Nyquist plot (where the negative equivalent series reactance $-X_s$ is plotted against series resistance R_s) is often used in electrochemistry and bioelectrical studies[McA96]. A Bode plot (a plot of the logarithm of the modulus of the measured impedance against the logarithm of frequency) highlights the frequency dependency of the impedance.

It is advisable to compare the fit between the experimental data and the impedance of a given model on both complex impedance and Bode plots to check the model's validity. It is common to plot only the imaginary parts against the frequency. This presentation of data has been criticized by McAdams [McA96]. It is highly recommended that the real part of the impedance or admittance should be also plotted in order to confirm the interdependence between the real and imaginary components.

2.6 Measurement Techniques

When describing analog instrumentation methods, it is useful to classify techniques according to the type of excitation functions employed, particularly with respect to the independent variable. For example, frequency domain impedance measurements are carried out using a small amplitude sinusoidal excitation with frequency as the independent variable. Alternatively, the pertubation and response may be recorded in the time domain with time as the independent variable, and the impedance as a function of frequency can then be extracted by time to frequency conversion techniques such as Laplace or Fourier transformation. Time domain methods typically use digital-processing techniques whereas frequency domain methods have traditionally used analog techniques, although digital processing is becoming common in synthesis and analysis of sinusoidal signals. [Mac87]

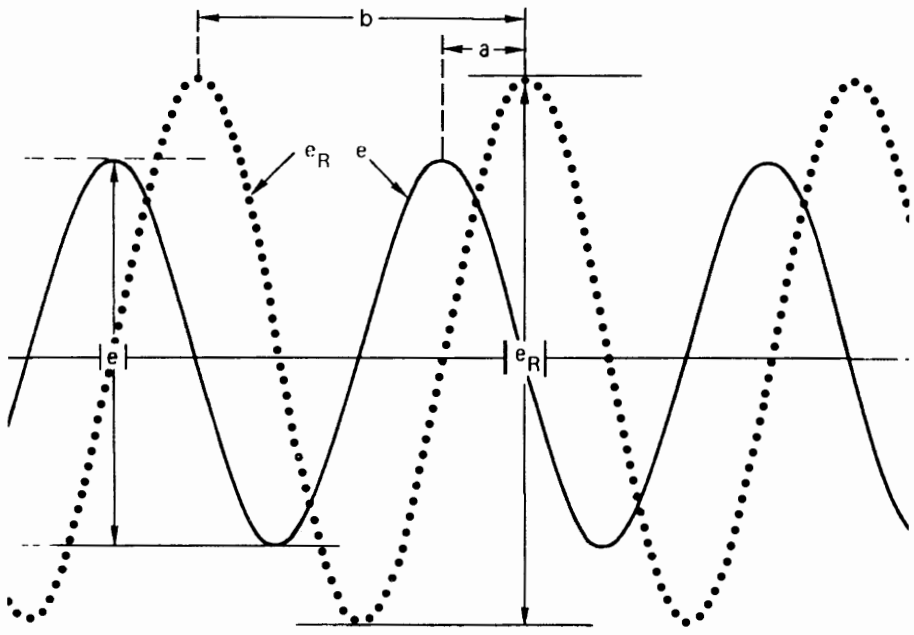

Figure 15: Direct impedance measurement with a two beam oscilloscope. e shows the applied voltage, e_R the resulting current.

2.6.1 Frequency Domain Methods

Audio Frequency Bridges

In the past, impedance measurements using reactively substituted Wheatstone bridges in the audio frequency range (i.e. between 20 Hz and 20,000 Hz) have been easiest to perform. The mathematics and methodology of such measurements are well understood. The upper frequency operating limit is imposed primarily by reactivity and the effects of stray capacitive shunts. In general, elimination of stray

capacitance is most important at high frequencies when measuring small capacitances or large resistances (i.e. for small area electrodes). The lower frequency limit which is typically about 20 Hz is determined by noise and non-linearity.

Oscilloscope Methods for Direct Measurement

By recording the applied voltage and the current on a two channel oscilloscope, the magnitude of impedance can be calculated from the ratio of the two peak-to-peak voltages and the directly observed phase angle. Figure 15 shows the two oscilloscope traces. This method can be used over a wide area of frequencies. The primary limitation is instrumental precision. On the one hand the linearity of the oscilloscope is seldom better than 1%, and it is difficult to measure phase angles directly with a precision better than 5 degrees.

Using a one beam oscilloscope, it is possible to estimate the impedance from Lissajous Figures. The plot of the applied potential vs. current, which opens another field: the cyclic voltammetry, which is also widely used for studying electrical properties of interfaces in [OL+94].

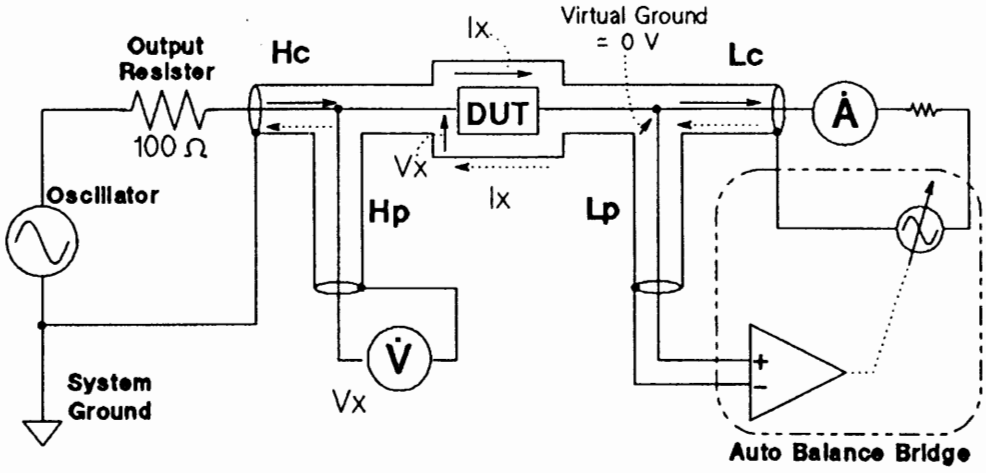

Figure 16: Four connection terminal measurement principle.

Automated Impedance Analyzers

An automated impedance analyzer operates with a so-called autobalance bridge. The instrument used in this work belongs to this class. The desired signal (comprising both ac and dc components) is applied to the unknown impedance or device under test (DUT) as shown in Figure 16. The current follower effectively constrains all the current flowing through the unknown impedance i_r to flow through the range resistor R_r, presenting a virtual ground at the terminal marked as low. For this condition the impedance can be measured as

$$Z_{unknown} = R_r \frac{e_i}{e_r}$$

The advantages of this method are the relatively high speed and high precision. This method is useable up to high frequencies. Since the in-phase and quadrature

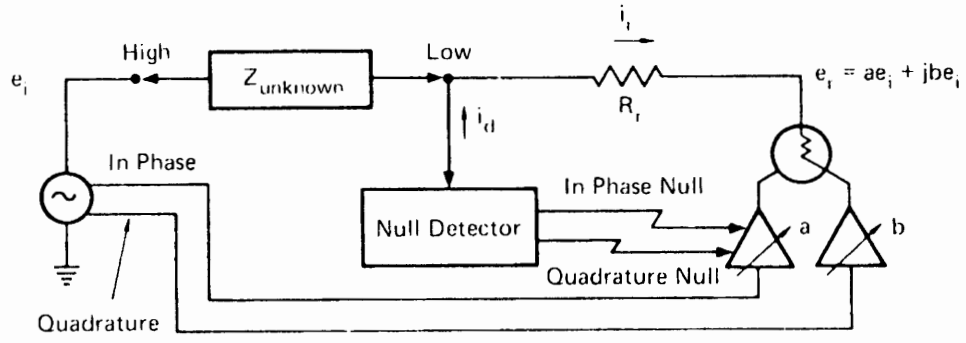

Figure 17: Schematic diagram of an autobalance bridge. The range resistor R is automatically adjusted to the system.

null signals usually derived from a PSD (phase sensitive detector), instruments of this type are limited at low frequencies due to the instability of analog filters with longer time constants [Mac87].The frequency range used in this work was between 20 Hz and 1 MHz.

2.6.2 Time Domain Methods

The impedance can be calculated from the pertubation response in the time domain, in which the excitation can be any arbitrary function of time. In principle, any of several linear integral transform methods can be used to convert from the time domain into the frequency domain, but the two most commonly used are Laplace and Fourier transforms:

$$F(s) = \int_0^\infty F(t)e^{st}dt$$

$$F(j\omega) = \frac{1}{2\pi}\int_{-\infty}^{\infty} F(t)e^{-j\omega t}dt$$

Any arbitrary time domain excitation can be used to measure the system impedance provided that the excitation is applied and the response recorded over a sufficiently long time to complete transforms over the desired frequency band.Thus, potential and current steps and various noise excitation patterns have been extensively used in the field of ac-polarography and corrosion science, especially for rapidly corroding systems.[Mac87]

For time-domain methods it is important to have a good analog-digital converter for the data acquisition and fast algorithms like the Fast Fourier Transform to obtain impedance spectra from the time domain.

Chapter 3

Materials and Methods

3.1 Materials

L-α or Egg-phosphatidylcholine (Egg-PC) at a concentration of 10 mg/ml, dissolved in chloroform was obtained from Avanti Polar Lipids, Alabaster, AL. Potassium chloride (KCl) were from Sigma Chemical Company, St. Louis, MO. n-Decane (goldlabel) used as a solvent of Egg-PC was fromAldrich Chemical Company, Milwaukee, WIS.

The teflon insulated silver wire (99.99% purity), stainless steel wire (AlSl 316 Fe/Cr18/Ni10/Mo3), platinum wire (99.99%) and copper wire were from Goodfellow Cambridge Limited, Cambridge, England. The wire data are summarized in Table 3.

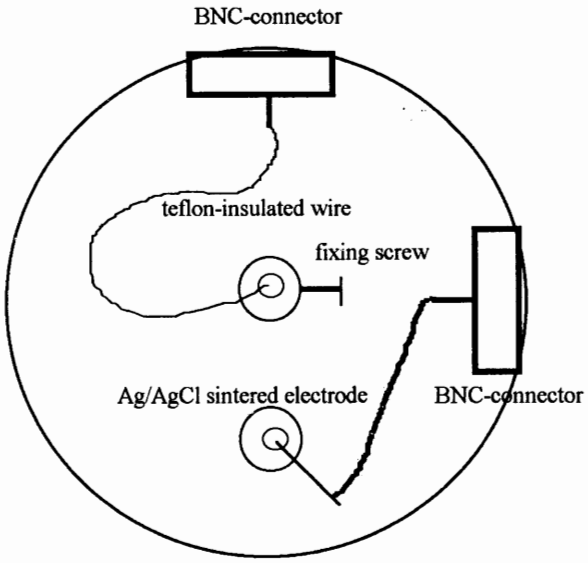

Figure 18: Schematic sketch of the electrode holder

conductor	conductor diameter	insulation thickness
Copper (Cu)	0.24mm	0.25mm
Platinum (Pt)	0.125mm	0.016mm
Stainless Steel	0.075mm	0.018mm
Silver (Ag)	0.25mm	0.024mm

Table 3: Properties of the teflon-insulated wires used in these studies

The cell measurements with bilayers took place in a 100ml beaker with a home-made electrode holder. Figure 18 shows the electrode holder.

3.2 Preparation of Lipids

The lipid bilayer forming solution was prepared using a method similar to that described by R. Murgosaova [M+95]. The lipids must first be purged of all chloroform. There are two steps in the procedure. The chloroform was first removed in about 15 minutes evaporated using a rotary flash evaporator (Buchler Instruments, Fort Lee, NJ) connected to a water-pump. To facilitate chloroform removal the flask containing the lipid solution was heated using a warm water bath (35°C) and the collector flask for the evaporated chloroform was cooled with ice. The evaporation of chloroform resulted in a thin lipid film in the flask. A mechanical pump was then used to pump the sample for at least one more hour at a pressure of about 0.1 torr. The lipids were then dissolved in n-decane to obtain a final concentration of 2.5% or 25mg lipids per 10 ml n-decane.

The final lipid solution was stored in 1ml flasks under nitrogen in the freezer.

3.3 LCR-Meter setup

For impedance measurements a HP 4284A Precision LCR Meter (20 Hz - 1 MHz) from Yokogawa-Hewlett-Packard, Japan, was used. The connection from the LCR Meter to the measuring cell was done with coaxial cables using four terminal connection.

Voltages applied to the bilayer lipid membrane formed on the tip of a teflon insulated wire were in the range from 10mV to 120mV. Voltages for the TiO_2 experiments were in the range from 10 mV to 1V.

The LCR Meter was connected to a DFI 80486 (33 MHz) computer via a GP-IB IEEE 488 bus. The experimental setup was controlled by a software, developed for this application. The LCR Meter was operated in the G-B (G conductance, B susceptance) mode, scanning the maximum possible frequency spectrum from 20 Hz to 1 MHz. Duplicate measurements were done for each frequency allowing the LCR-meter to stabilize.

3.4 Lipid Bilayer Experiment

The measuring cell consisted of 100 ml glass beaker, electrode holders and BNC connectors, see Figure 18. The Ag/AgCl sintered electrode was used as the counter electrode. The measuring electrode was the teflon insulated wire.

The preprepared membrane forming solution was taken out from the freezer at least one hour before use in order to prevent water condensation. Using a disposable pipette a drop of the lipid solution was deposited into a little bowl. The end of the teflon insulated wire was totally inserted into this drop of lipid solution and cut with a scalpel. This assured that the lipid solution was in direct contact with the freshly

cut metal. The wire was left in this position 1 - 2 minutes and then immediately immersed in the aqueous KCl solution in the beaker.

3.5 Preparation of TiO_2 films on conductive glass

A stripe of conductive glass (8 cm long, 4 cm wide) was fixed to the table with adhesive tape, leaving a a stripe 2 cm wide on the conductive glass, leaving noncoated areas for electrical contact. A first layer of TiO_2 was brought on the glass to form a solid, isolating TiO_2-film using Titanium(IV)butoxide. A TiO_2 suspension was used to built the colloidal layer. The preparation of the suspension was done as described in [N+93]. The pulverized TiO_2 powder (6g), which consists of aggregated particles, was ground in a porcelain mortar with a small amount of water (2ml) containing acetylacetone (0.4ml) to prevent reaggregation of the particles. After the powder had been dispersed by grinding in a viscous paste, it was diluted by slow addition of water (8ml) under continued grinding. Finally a non-ionic surfactant (Triton X-100) was added to facilitate the spreading of the colloid on the substrate. The colloid was applied on one of the free edges of the conducting glass and distributed with a glass rod sliding once (!) over the tape covered edges. After air drying the adhesive tape was removed and the preparation was placed in an oven at 450-550 °C for 30 minutes. The resulting conductive glass covered with a TiO_2 strip was cut in pieces. Each piece contained an area of 1 cm^2 of TiO_2-substrate.

3.6 Setup for the TiO_2 based solar cell experiments

The piece of conductive glass with or without TiO_2-film was fixed in a holder. The other electrode, a piece of a Pt foil ($1cm^2$) was pressed with a piece of glass against the conductive glass covered by the TiO_2 film. For a defined distance between the glass and the Pt-electrode a small plastic spacer was used.

The LCR-meter was connected to the solar cell by means of a BNC-connector holder. Two cables were used to connect the LCR meter to the cell. One cable was fixed with a cable lug to the holder which was in contact with the conductive glass. The other cable had an alligator clip which was connected to the Pt-electrode.

For the solar cell application, the TiO_2 had to be dyed with porphyrins. The TiO_2 -electrode was put in the porphyrin solution overnight for 15 hours.

3.7 Data Analysis

The data analysis was found to be challenging because the admittance spectra based on simple equivalent circuits such as that shown in Figure 13 could not simultaneously fit the frequency dependence (20Hz - 1MHz) of the real and imaginary part of the system admittance. It was found that a good fit in the admittance spectrum did not necessarily result in a good fit in the impedance plane. Only a good fit in

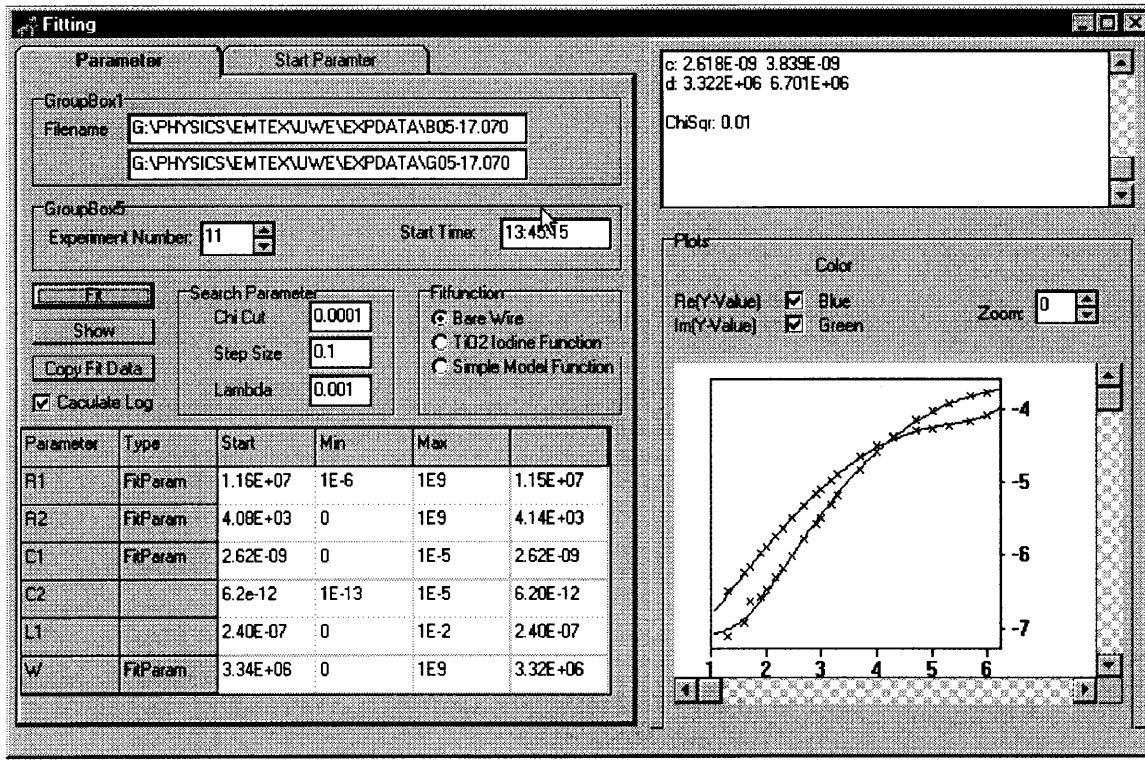

Figure 19: Graphical Interface of the used fitting software. The program uses the Marquardt algorithm to perform a complex, non-linear least square fit with up to 6 parameters.

both the real and imaginary part of admittance or impedance will result in good fits in all graphical representations.

For these reasons a Complex Nonlinear Least Square (CNLS) fit using Marquardt algorithm was used for data analysis. The real and imaginary part were equally weighted. The concepts of CNLS are described in [Mac87]. Laboratory software written in Delphi (an object oriented version of Pascal) was written making it possible the fit different functions defined by the equivalent circuits for experimental

data. Some circuits are simply a subset of a more complex circuit. In the present form the program allows up to 6 different independently variable elements in the circuit. The raw data and the fitted function in both real and imaginary parts are plotted using the logarithmic frequency scale. The admittance can be using either linear or logarithmic scales. Figure 19 depicts the graphical interface of the CNLS software for Windows 95.

3.8 Admittance spectra of discrete element circuit

The performance of the LCR-meter, data acquisition and data analysis software, was tested using RC circuits. The values of resistors and capacitors were chosen in such a way to cover the range of expected values. It was also observed that single values of components were frequency dependent, the capacitance, for example had a resistive component at high frequencies. As it can be seen, though, the experimental data fit very well.

In Figure 20 we illustrate the frequency dependence of conductance and susceptance of a prototype RC circuit (Figure 13) corresponding to membrane formed at the tip of the teflon insulated wire: membrane capacitance, $C_1 = 300pF$, membrane resistance, $R_1 = 95k\Omega$ and access resistance $R_2 = 4800\Omega$.

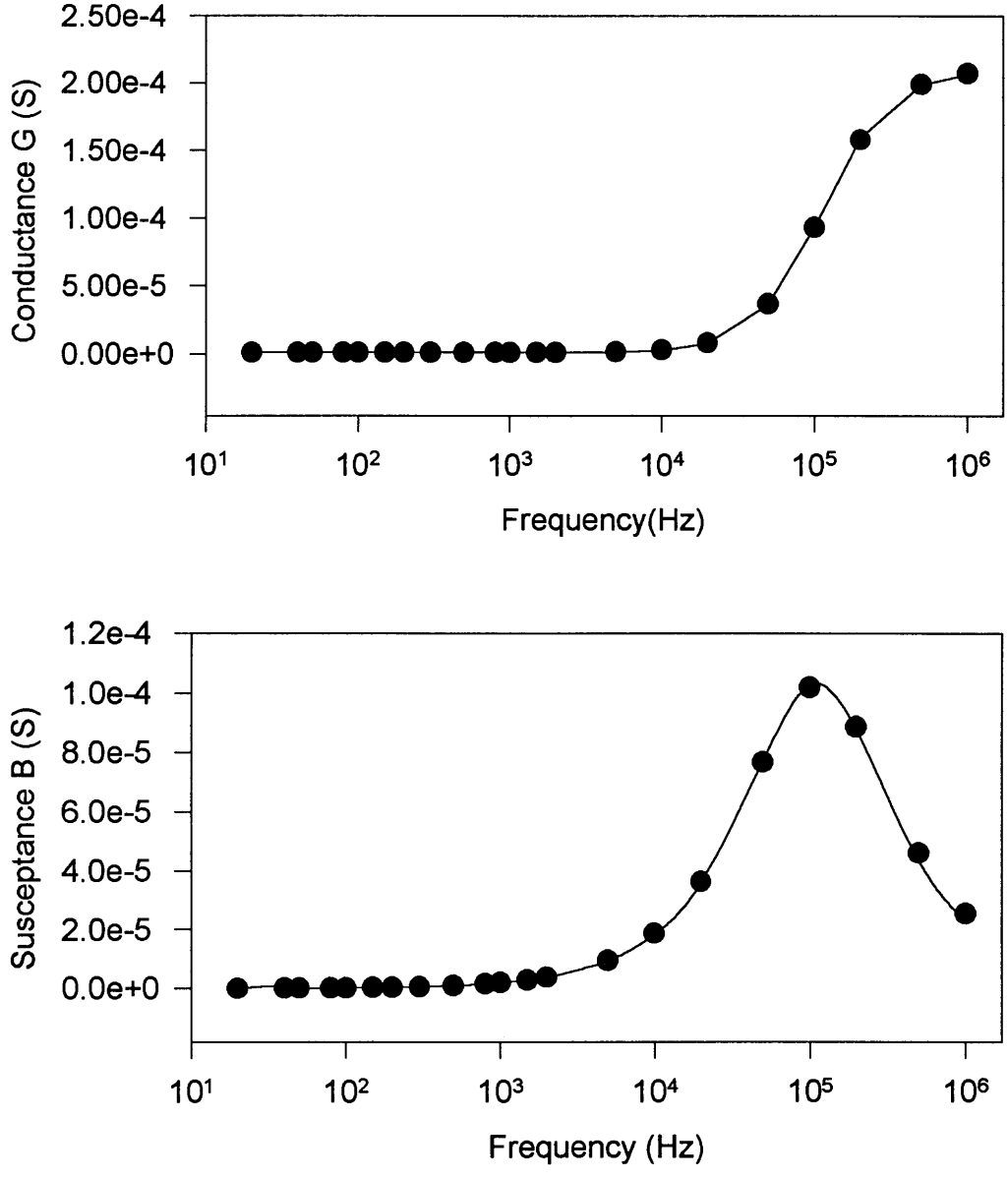

Figure 20: Admittance spectra of a circuit built with discrete elements. A measurement of the real values: $R_1 = 95k\Omega$, $R_2 = 4800\Omega$, $C_1 = 300pF$. The fitted values are $R_1 = 94k\Omega$, $R_2 = 4800\Omega$, $C_1 = 300pF$. The solid curves illustrate the frequency dependence of a circuit conductance and susceptance predicted for RC values obtained by the least square fit method.

Chapter 4

Results and Discussion

4.1 Characterization of Bilayer Lipid Membranes

Equivalent RC circuits have been used to analyze and discuss the electrical properties of lipid membranes, electrodes, self-assembled monolayers and lipid bilayers on electrodes [S+96] [WT90] [MT91] [OL+94] [OT97].

The charged interfaces, such as lipid bilayer formed on the tip of metallic wire [OL+94], or lipid bilayer formed on the alkanethiol monolayer supported by the gold surface have been represented by the prototype equivalent circuit shown in Figure 13. In this representation the capacitor C_1 represents the capacitance of the electrical double layer, resistor R_1 parallel with C_1 is the resistance associated with the transfer of charge across the interface and resistor R_2 represents the resistance

of solution and conductors. We found in preliminary studies that frequency spectra of admittance of wires with and without lipids cannot be predicted using prototype circuits such as that shown in Figure 13. For this reason we measured admittance spectra of elements comprising the measuring cell, individually and in combinations. These studies included

- Two sintered Ag/AgCl electrodes immersed in KCl solution. The purpose of these studies is to determine the equivalent circuit for the reference electrode. One Ag/AgCl electrode is used as the reference electrode when measuring properties of lipid films and of cut bare wires.

- Measuring cell with KCl solution in which the length of immersed teflon insulated wire was varied. The purpose of this study was to determine the effect of stray and inter-electrode capacitance on the admittance spectra.

- Cut teflon insulated wires were used as supports for self-assembled lipid films. The purpose of these studies was to obtain admittance data needed to recognize the presence or absence of the lipid film at the tip of the wire and to derive equivalent circuit for this experimental configuration.

- Teflon insulated wires with lipid films formed at the tips of the wires which were the systems of interest.

4.1.1 Admittance spectra of two Ag/AgCl electrodes

The frequency dependence of conductance and susceptance of two Ag/AgCl electrodes measured in 0.1 M KCl solution is shown in figure 21. The conductance, G, monotonously increased from 0.024 Siemens to the limiting value at high frequency of approximately 0.0295 Siemens. The 90° out of phase admittance monotonously decreased from 0.004 Siemens and became negative at frequencies above 100 kHz suggesting the presence of self inductance in the measuring circuit. The separation of Ag/AgCl electrodes was about 2 cm. No voltage dependence was observed for an applied voltage between 10 - 120 mV.

The experimental admittance spectra cannot be explained in terms of a simple circuit consisting of linear elements such as resistors and capacitors as depicted in the prototype circuit of Figure 13. It was necessary to incorporate nonlinear elements into the circuit. The solid curves shown in Figure 21 illustrate the predictions of an equivalent circuit in which each interface of Ag/AgCl electrode is represented by a Warburg-type impedance in series with an ohmic resistor representing the KCl solution. The value of lumped circuit parameters obtained from the best fit curves were as follows; the parameter $\sigma = 75\Omega s^{-\frac{1}{2}}$ (σ defines the Warburg-type impedance), the series resistance $R_2 = 34\ \Omega$, and the self-inductance $L = 0.24\ \mu H$.

It should be pointed out that simple RC circuits, without the presence of Warburg-type impedance element, were found to be applicable to mercury drop

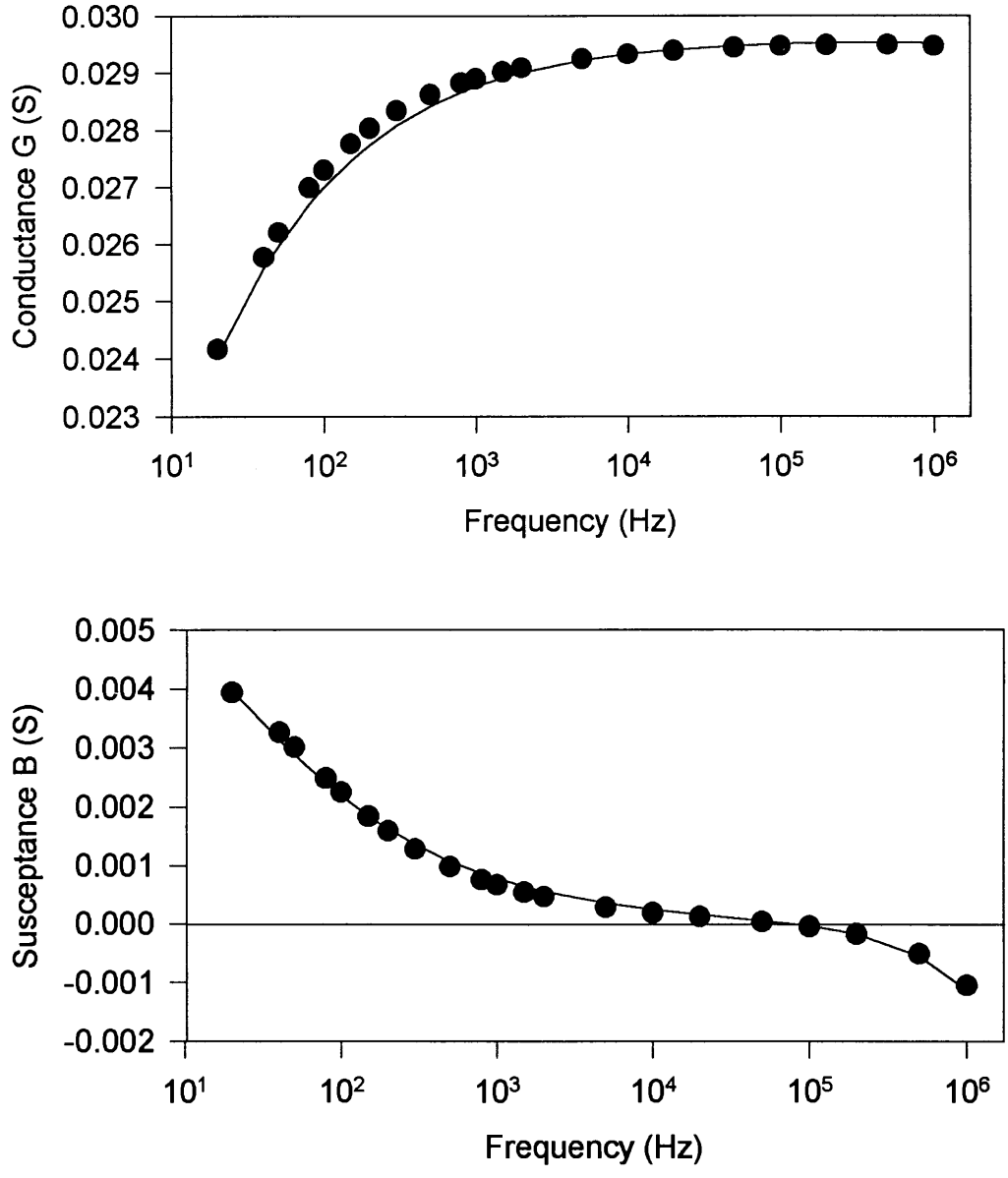

Figure 21: Admittance spectra of two Ag/AgCl electrodes in 0.1M KCl. The symbols show the measured values and the solid curve illustrates the prediction obtained for the equivalent circuit which consists of Warburg impedance σ in series with a resistor R_2 and an inductor L_1. The Warburg impedance represents the electrode/aqueous solution interface, the series resistor represents the access and solution resistance, and the inductor the cable self-inductance. The least square fit values of the parameters were $\sigma = 75\ \Omega s^{-\frac{1}{2}}$, $R_2 = 33.8\ \Omega$and $L_1 = 0.24\ \mu$H.

electrode suspended in ammonium fluoride solution [AR71]. For the mercury electrode the capacitance was found to decrease with frequency at frequencies above 20 kHz. The effect was associated with the kinetic limitations of charging and discharging the diffuse double layer at the surface of mercury electrode at high frequencies.

The suspended mercury hemispherical electrode represents an ideal electrode: (i) it has a perfectly clean and smooth surface, and (ii) it is a "blocking" electrode without charge transfer across the interface. For these reasons it can be represented by the prototype equivalent circuit (Figure 13) omitting resistor R_1. In contrast, our Ag/AgCl electrode is (a) sintered and therefore porous (which for our application is desirable), and (b) is not blocking. The Ag/AgCl electrode can support a high rate of interfacial charge transfer of silver and chloride ions. The net conductance of the two-electrode circuit in 1 M KCl was high, about 30 mS.

A survey of the literature indicates that the impedance of common electrodes such as Pt are not well understood processes. Schwan [Sch67] pointed out that electrodes with excellent dc-characteristics regarded as "nonpolarizable", are not necessarily suitable for transient and ac-studies. Schwan employed a series RC circuit similar to one used in studies with the mercury electrode to describe the Pt-electrode polarization impedance. However this circuit was inadequate for the Pt electrode since Schwan found that the R and C values decrease with frequency

(in the experimental range of 20 Hz to 200 kHz). The Pt electrode (area 1.4 mm^2) in saline solution can be characterized by a frequency dependent resistor

$$R(f) = R_0 f^{-0.51}$$

where $R_0 = 750\Omega$ and a frequency dependent capacitance

$$C(f) = C_0 f^{-0.37}$$

where $C_0 = 71.2\mu F$. The physical origin of the frequency dependence was not discussed.

The origin of Warburg-type impedance in the present Ag/AgCl system (Figure 21) is not clear but several mechanisms can be proposed. First, it is known that rapid kinetics of charge transfer across the electrode/solution interface would create local concentration gradients whose magnitude depend on the frequency. The solution of the electrodiffusion equation predicts a frequency dependent conductance and susceptance [SRS70]. Since the Ag/AgCl electrode is not of the "blocking" type and since oxidation and reduction processes are taking place at the electrode surface, it is conceivable that the frequency dependence predicted by Equation 2 and the fit of our equivalent circuit model to the data indicate the presence of diffusion limited charge transfer at the surface of Ag/AgCl electrode.

A second possible mechanism explaining the presence of the nonlinear element in the equivalent circuit can be associated with electrode porosity. It was shown that

the distribution of faradaic and displacement currents within pores is frequency dependent [dL67] and cannot be modeled by discrete circuit elements. At low frequencies the current penetrates through the pores and all pore surfaces can be charged. The current penetration into the pore decreases with the increasing frequency. This mechanism was demonstrated for porous carbon electrodes. [Rai90]

Third possible origin of Warburg-type impedance can be associated with the electrode roughness. The effect of roughness on a scale from 0.01 to 100 μm was discussed by de Levie [dL90] in terms of the fractal properties of the electrode surface. De Levie has shown how the charge transfer coefficient at the electrode surface depends on the electrode roughness. Electrode roughness results in an impedance element similar to the Warburg-type impedance used in this study to fit the data (Figure 21). The theoretical curves are the admittance spectra of an equivalent circuit consisting of a Warburg impedance element in series with a pure resistor. The inductance in series stands for the inductance in the cables. Its value of 0.24μH is in the range of self inductances for a short circuit system. The presence of self-inductance becomes noticeable at frequencies above 50 kHz. A parallel stray capacitance can be included but has no measureable effect in the frequency range below 1 MHz. Also, the experimental data suggest the absence of a capacitance for the double layer as predicted in the Randles' circuit in Figure 24 as described by Sluyters [SRS70].

The value of the Warburg impedance σ was found to be around 75 $\Omega s^{-\frac{1}{2}}$. The theoretical prediction for σ leads to a value of 1.1 $\Omega s^{-\frac{1}{2}} cm^2$. This gives us a theoretical surface area of 1.5mm^2, which is about an order of magnitude too small.

Another approach explaining nonlinear interfacial impedance is described by de Levie and Vogt [dLV90]. De Levie has shown that a theoretical model based on the fractal properties of electrode surface predicts half-cell impedance given by

$$Z_{hc} = R_s + \frac{1}{b}\left(\frac{R_{ct}}{1 + i\omega R_{ct} C}\right)^{\xi}$$

where R_s stands for the solution resistance, R_{ct} for the charge transfer resistance, and C for the interfacial capacitane, and b is used as a geometrical factor. The coefficient ξ describes the degree of roughness of the interface. For a value of $\xi = \frac{1}{2}$ and $b = 1$ this term becomes equivalent to the Warburg impedance as given in Equation 1 and our equivalent circuit used to fit the data with $R_s = R_1$, $R_{ct} \to \infty$ and $C = \sigma^2$. A value of $\xi = \frac{1}{2}$ is applicable for a porous electrode such as the sintered Ag/AgCl-electrode used in this study. [dLV90]

4.1.2 Stray and inter-electrode capacitance

In order to develop an equivalent circuit of self-assembled bilayer lipid membrane it is necessary to characterize the admittance of the measuring cell and electrodes. The electrode system consists of the teflon insulated wire and the Ag/AgCl electrode. The teflon insulated wire on which the lipid membrane is formed acts as a cylindrical

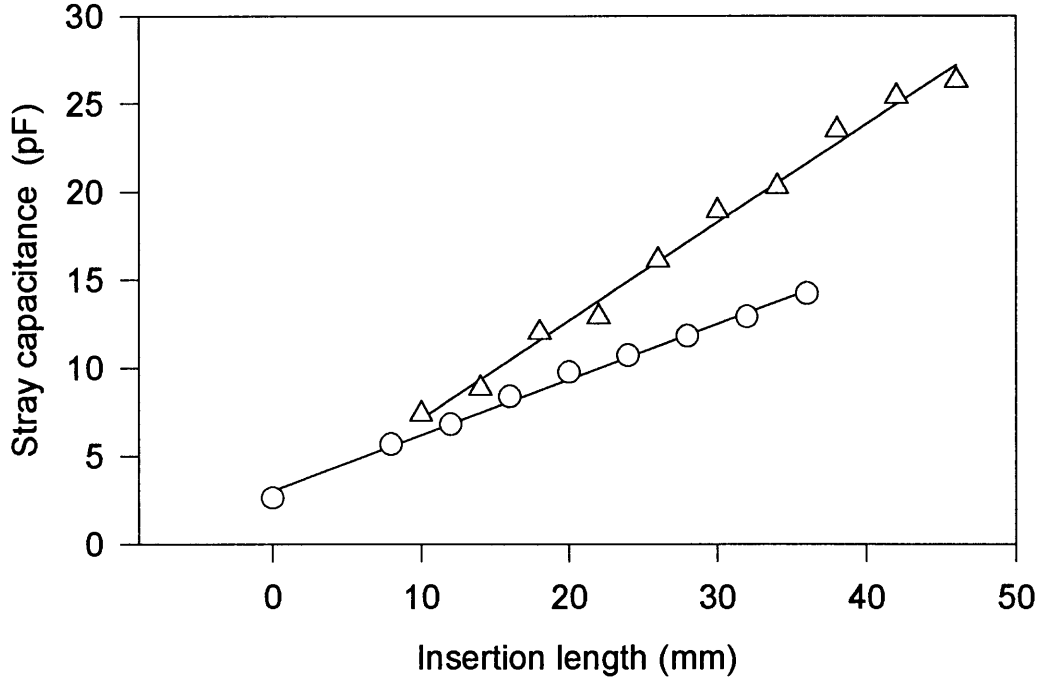

Figure 22: The effect of insertion length of the teflon insulated wire versus the equivalent stray and interelectrode capacitance. The plot of capacitance C_2 as a function of the wire insertion length in 0.1 M KCl; for steel wire (◯) and silver wire (△). The applied voltage was 50mV. The data symbols illustrate the measured values and the straight line is the fit of the equation for cylindrical capacitor.

capacitor when immersed in a conductive electrolyte such as the 0.1M KCl solution used in these studies with membranes.

We measured the frequency dependence of conductance and susceptance of teflon insulated steel and silver wires as a function of insertion length. The teflon insulated wire was formed into a loop and during the insertion length measurements the

uncoated end of the wire was not immersed to avoid measuring conductance through the uncoated wire end.

Due to the teflon insulation the conductance was not measurable and was compareable or below the instrument sensitivity limit, $G \leq 10^{-9}S$. The stray and inter-electrode capacitance, C_2, was obtained from the measured susceptance according to

$$C_2 = \frac{B}{2\pi f} \tag{4}$$

The dependence of C_2 on the depth of immersion length is shown in Figure 22. The experimental results indicate a linear relationship between the equivalent capacitance and the depth of immersion, the length of a cylindrical capacitor.

The data in Figure 22 can be understood in terms of the following model for the total equivalent capacitance C_2. Two contributing terms to the stray capacitance are assumed, (i) a stray capacitance C_0 accounting for the cables and the geometric capacitance of electrodes in air and (ii) the cylindrical capacitor corresponding to the segment of the teflon insulated wire immersed in the electrolyte.

For a very thin teflon layer the capacitance can be written as

$$C = C_0 + \epsilon_r \epsilon_0 \frac{A}{d} \tag{5}$$

where $A = 2\pi rl$ is the exposed area of the immersed wire in the electrolyte, r is the radius of the wire, d is the thickness of the insulation and l is the immersion length.

[KCl] ($\frac{mol}{l}$)	Spec. conductivity ($\frac{1}{\Omega m}$)
1	11.19
0.1	1.289
0.01	0.1413
0.001	0.01469
0.0001	0.001489

Table 4: The specific conductivity of the KCl solutions used in these studies. The values are adapted from reference [DA75]

Electrode	Diameter	R_{access} for 0.1M [KCl]	R_{access} for 1M [KCl]
steel-teflon	0.075 mm	5172 Ω	596 Ω
Ag - teflon	0.25 mm	1552 Ω	179 Ω

Table 5: The access resistance for the steel and silver wires used in these studies. The values were calculated from Equation 3.

4.1.3 Characterization of teflon insulated wires used as electrodes

It was found necessary to study the admittance spectra of cut teflon insulated wires in a KCl solution as the prerequisite for a better understanding of lipid membranes. Both wires, the teflon-insulated steel and silver teflon-insulated wires, were cut and immediately immersed in KCl solution to characterize the system without the membrane. In this case the wire works as the counterelectrode. Since the diameters of the wires used were very small, effects associated with the presence of access resistance were expected.

The objective of these studies with the cut wire was to arrive at an equivalent circuit for the interface between the cut wire and the electrolyte. The admittance

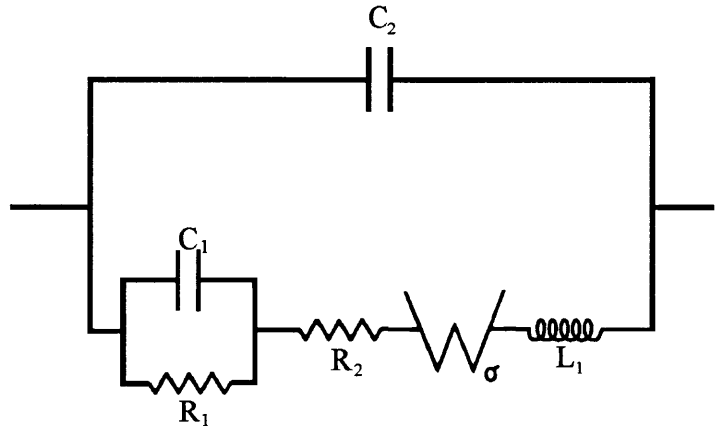

Figure 23: Equivalent circuit used for fitting the data. C_2 represents the stray capacitance of the wires, L_1 the self inductivity. C_1, R_1 and R_2 are representing the classical interface. The Warburg impedance σ was included for diffusion processes.

spectra of the steel wire and silver wire are shown in Figures 25 and 26. In both cases it was not possible to fit the measured spectra with a simple interface model similar to the one in Figure 13. It was necessary to introduce a Warburg-type impedance, a self-inductance and a stray capacitance. Using this extended circuit, shown in Figure 23, it was possible to fit the data obtained for the steel wire and for the silver wire for times shortly after immersion in the 0.1 M KCl solution. This anomalous behavior of the silver wire can be attributed to corrosion processes. Two points support this:

1. The admittance spectra changed with time which is characteristic for corrosion processes.

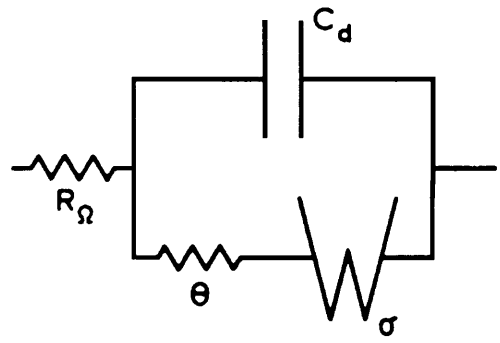

Figure 24: Randles' equivalent circuit. θ, transfer resistance; W_σ, Warburg impedance; C_d double layer capacity; R_Ω, ohmic resistance [SRS70]

2. Visible changes of the wire surface was observed: The tip of the wire became black whereas before the immersion it was metallic grey. It was found that this corrosion extended approximately 5 mm beneath the teflon insulation coating.

The admittance spectra of cut teflon insulated steel and silver wires (shown in Figures 25 and 26) are qualitatively similar in that both the conductance and susceptance increases with frequency. However, the magnitudes of changes are very different. Within the frequency range 20 Hz - 1 MHz, the parameters for the steel wire change 2-3 orders of magnitude, whereas those for the silver wire change by about one order of magnitude. The solid curves illustrate the fit of the simplest equivalent circuit that can reproduce the measured admittance spectra. The optimal least square fit parameters are given in the respective figure captions.

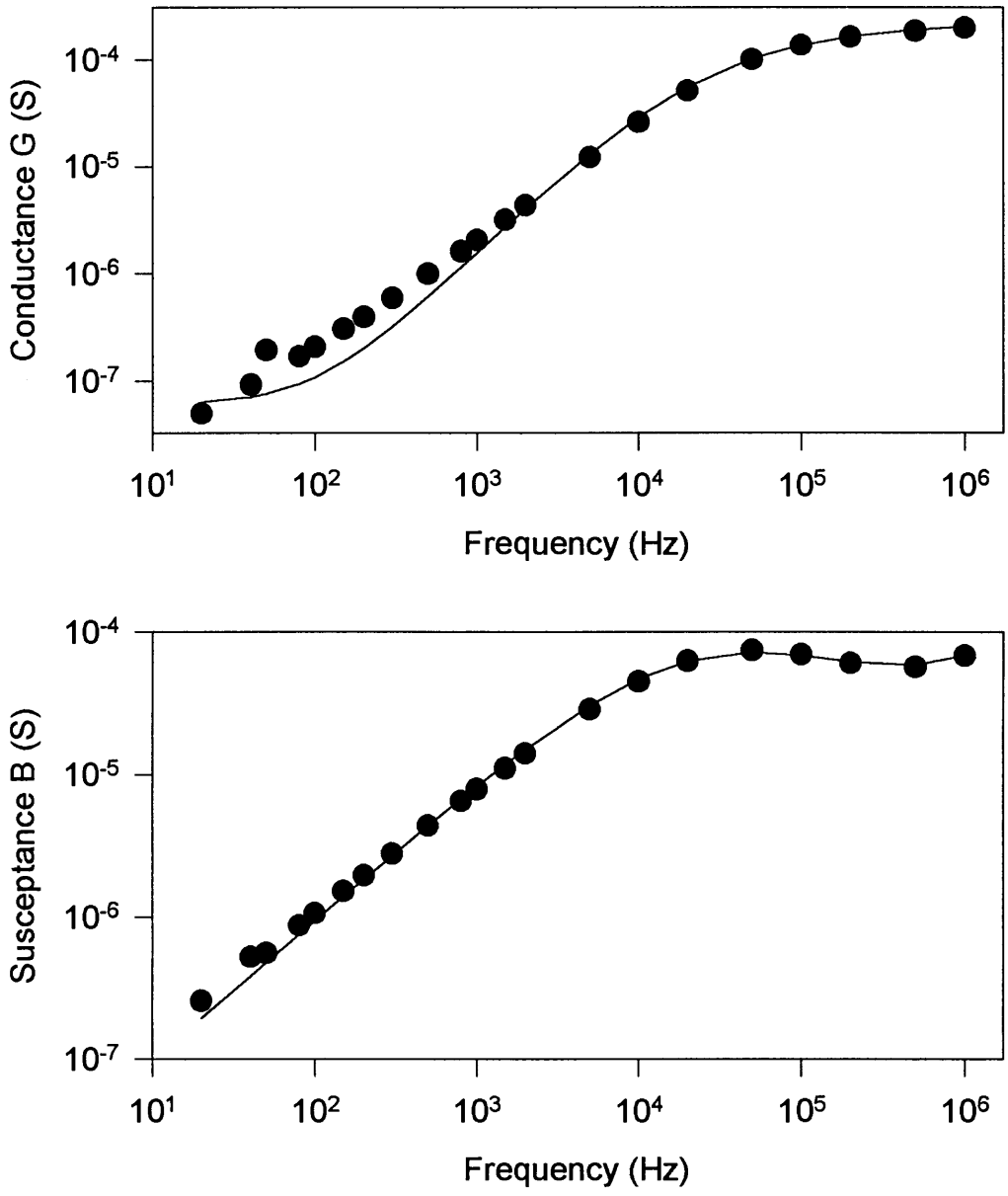

Figure 25: The admittance spectra of teflon insulated steel wire immersed in 0.1M KCl solution after 13min at 50mV. The circuit shown in Figure 23 was used for the curve fit. A self-inductance of $L_1 = 0.24\mu H$, resulting from the cables and a stray capacitance of $C_2 = 6.2$ pF, was determined. The other values are $R_1 = 17.8M\Omega$, $R_2 = 4040\Omega$, $C_1 = 2.11$nF, and $\sigma = 2.13\ M\Omega s^{-\frac{1}{2}}$

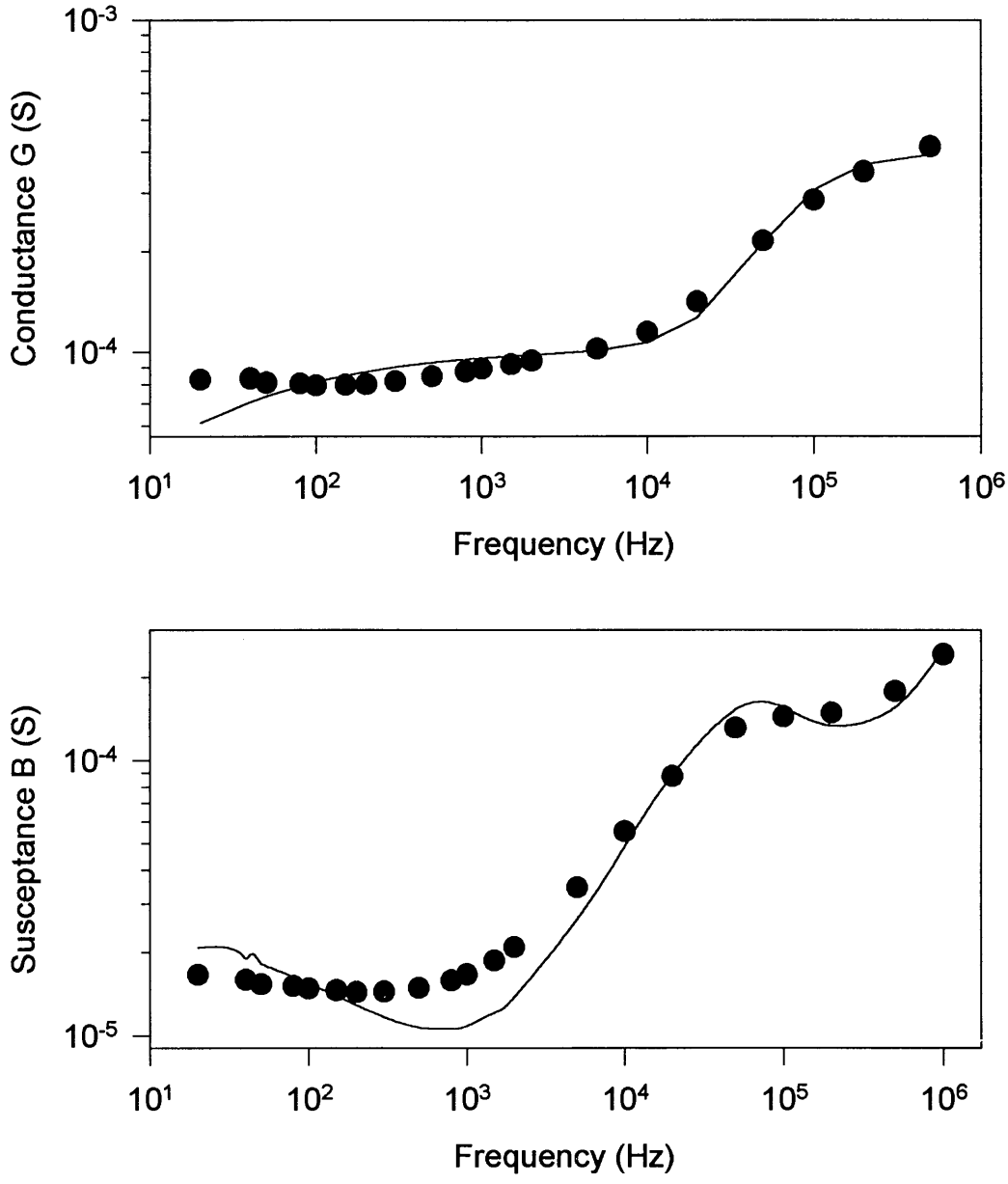

Figure 26: The admittance spectra of the teflon insulated silver wire immersed in 1M KCl solution after 43min at 70mV. The circuit shown in Figure 23 was used to fit the curve. The fitted values are: R_1=7150Ω, R_2=2440Ω, C_1=1.39nF, C_2=37.2pF, L_1=0.24μH, and σ=5.54M$\Omega s^{-\frac{1}{2}}$.

time (min)	R_1 (MΩ)	R_1 (Ωcm^2)	R_2 (Ω)	C_1 (nF)	C_1 ($\frac{\mu F}{cm^2}$)	σ ($M\Omega s^{-\frac{1}{2}}$)	σ ($\Omega s^{-\frac{1}{2}} cm^2$
3	10.3	455	3940	1.88	42.6	1.89	83.5
13	17.8	764	4040	2.11	47.8	2.13	94.1
24	9.68	428	4140	2.15	48.7	2.18	96.3
34	11.2	495	4170	2.29	51.8	2.14	94.5
45	12.4	548	4190	2.39	54.1	2.56	113
55	14.6	645	4220	2.44	55.2	2.68	118
66	13.0	574	4230	2.45	55.5	2.70	119
110	10.1	446	4190	2.53	57.3	3.14	139
120	12.2	539	4180	2.56	57.9	3.23	143
131	12.7	561	4200	2.53	57.3	3.23	143

Table 6: The time dependence of fitted values for a teflon insulated steel wire at 50mV. The time is measured after the freshly cut wire is immersed in 0.1M KCl solution. Values for C_2 (stray capacitance) and for L_1 (self inductance of cables) were set to 6.2pF and 0.24μH.

The admittance spectra were measured over a period of several hours. Two notable features of the experimental results are that (i) the admittance spectra of both steel and silver wires changed with time and (ii) at later times it was not possible to fit the silver wire spectra with the equivalent circuit shown in Figure 26. In view of these properties it is only meaningful to discuss data obtained with the steel wires.

Insight into the changes taking place in the steel wire system can be gained from an inspection of the time dependence of the values of the equivalent circuit elements given in Table 6 and from the voltage dependence of the circuit elements in Table 7.

Voltage (mV)	R_1 (MΩ)	R_1 (Ωcm^2)	R_2 (Ω)	C_1 (nF)	C_1 ($\frac{\mu F}{cm^2}$)	σ ($M\Omega s^{-\frac{1}{2}}$)	σ ($\Omega s^{-\frac{1}{2}} cm^2$)
10	17.1	755	3900	1.77	40.1	1.97	**87.0**
20	12.6	557	3930	1.82	41.2	1.90	**83.9**
50	10.3	455	3940	1.88	42.6	1.89	**83.5**
70	12.7	561	3930	2.01	44.8	1.98	**87.5**
80	13.4	592	3950	2.07	46.9	2.02	**89.2**
100	14.7	649	3940	2.21	50.0	2.08	**91.9**
120	9.71	429	3980	2.30	52.1	2.03	**89.7**

Voltage (mV)	R_1 (MΩ)	R_1 (Ωcm^2)	R_2 (Ω)	C_1 (nF)	C_1 ($\frac{\mu F}{cm^2}$)	σ ($M\Omega s^{-\frac{1}{2}}$)	σ ($\Omega s^{-\frac{1}{2}} cm^2$)
10	7.21	319	4100	1.91	43.2	1.92	84.8
20	11.2	495	4030	2.06	46.6	2.09	92.3
50	17.8	786	4040	2.11	47.8	2.13	94.1
70	9.32	412	4060	2.17	49.1	2.13	94.1
80	11.5	508	4040	2.25	50.9	2.20	97.2
100	10.2	451	4060	2.34	53.0	2.19	96.8
120	10.7	473	4060	2.47	55.9	2.22	98.1

Voltage (mV)	R_1 (MΩ)	R_1 (Ωcm^2)	R_2 (Ω)	C_1 (nF)	C_1 ($\frac{\mu F}{cm^2}$)	σ ($M\Omega s^{-\frac{1}{2}}$)	σ ($\Omega s^{-\frac{1}{2}} cm^2$)
10	14.3	632	4170	2.40	54.3	3.30	146
20	21.4	945	4110	2.54	57.5	3.38	149
50	14.3	632	4140	2.58	58.4	3.32	147
70	11.5	508	4140	2.62	59.3	3.32	147
80	12.4	548	4150	2.64	59.8	3.30	146
100	11.9	526	4150	2.72	61.6	3.29	145
120	10.2	451	4140	2.84	64.3	3.29	145

Table 7: The voltage dependence of fitted values for steel wire immediately after immersion in 0.1M KCl, 10 minutes later and after 130 minutes. Values for C_2 (stray capacitance) and for L_1 (self inductance of cables) are fixed at 6.2pF and 0.24μH.

Considering the values and properties of the equivalent circuit elements it is possible to assign them the following physical significance and to describe the interface as follows:

- The resistance R_2, which was found to be independent of time, represents the access resistance to the cut wire surface. The measured value $R_2 = 4150 \pm 91\Omega$ is close to the theoretically predicted value of 5200 Ω (Table 5).

- The capacitance C_1 and the resistance R_1 represent the interface of the steel wire. C_1 can be identified as the diffuse double layer capacitance since its value, normalized to unit surface, yields a value of the order of 50 $\frac{\mu F}{cm^2}$. Resistance R_1, having a characteristic value of the order of 10 MΩ, represents the charge transfer resistance.

- The Warburg-type impedance element most likely reflects the roughness and diffusion limitation within the interfacial region of the cut wire. The parameter σ of the Warburg-type impedance was found to be equal to 2-3 M$\Omega s^{-\frac{1}{2}}$ while its value normalized to the electrode surface area was comparable (within a factor of two) to the Warburg-type impedance found for the two electrode Ag/AgCl system. In view of the above properties one can characterize the cut stainless steel wire as a partially blocking electrode.

- The time dependence of the fitting parameters suggest that the interface of the cut stainless steel wire is not inert. The corrosive process resulted in an increase (by less than factor of two) of the capacitance C_1 and the Warburg-type impedance. This time dependent effect may be associated with the growth of the interface underneath the teflon insulation as corrosion of the teflon insulated silver wire was found to extend 5 mm underneath the teflon coating.

The effect of applied ac voltage was found to be minor. Only capacitance C_1 was found to be voltage dependent which is in agreement with associating C_1 with the diffuse double layer capacitance. Diffuse double layer capacitance is known to be voltage dependent. [BCY80]

Corrosion processes are very complex. A model for corrosion of the silver wire is discussed by Bockris [WBCY80] and includes 28 parameters. Another model is presented by Jüttner [Jüt90]. The interface is assumed to be a multi-layer system. Each layer is described by a resistance in parallel with a capacitor. Defects are simulated by parallel interfaces. In this study a double layer capacitance increasing with time was found with a value of around 30 $\frac{\mu F}{cm^2}$.

Our results of admittance spectra of cut teflon insulated stainless steel and silver wires suggest that silver wire may not be suitable as support for the self-assembled lipid membranes because of the instability of the interface.

4.1.4 Bilayer Lipid Membrane Characterization

Bilayer lipid membranes were formed on the tip of the teflon inslulated wires after cutting the wire in membrane forming solution and immersion in 0.1 M KCl. The measurements of admittance spectra was inititated shortly after the immersion so it was possible to characterize the wire with the deposited lipid film from approximately 30 seconds after the immersion up to several hours, in 10 minutes intervals. The objective of these studies was to follow the membrane formation process, obtain information on stability of the membrane, stability of the membrane properties, and to develop understanding of the membrane properties in terms of equivalent circuits.

First of all, the presence of a lipid film on the cut wire was detectable as a change in the admittance spectrum as compared to that of bare wire. Typical admittance spectra of silver and steel wires with lipid films are shown in Figures 27 and 28, respectively. Both spectra are qualitatively and quantitatively similar. Both the conductance and susceptance monotonously increase with the frequency and the changes of admittance components represented 3-4 orders of magnitude in the frequency range from 20 Hz to 1 MHz. Attempts to fit the measured spectra using the prototype interface circuit shown in Figure 13 failed. The solid curves in Figures 27 and 28 illustrate the predictions based on the equivalent circuit used to fit the experimental data for bare wires. The least square fit parameters are given in Tables 8 - 11.

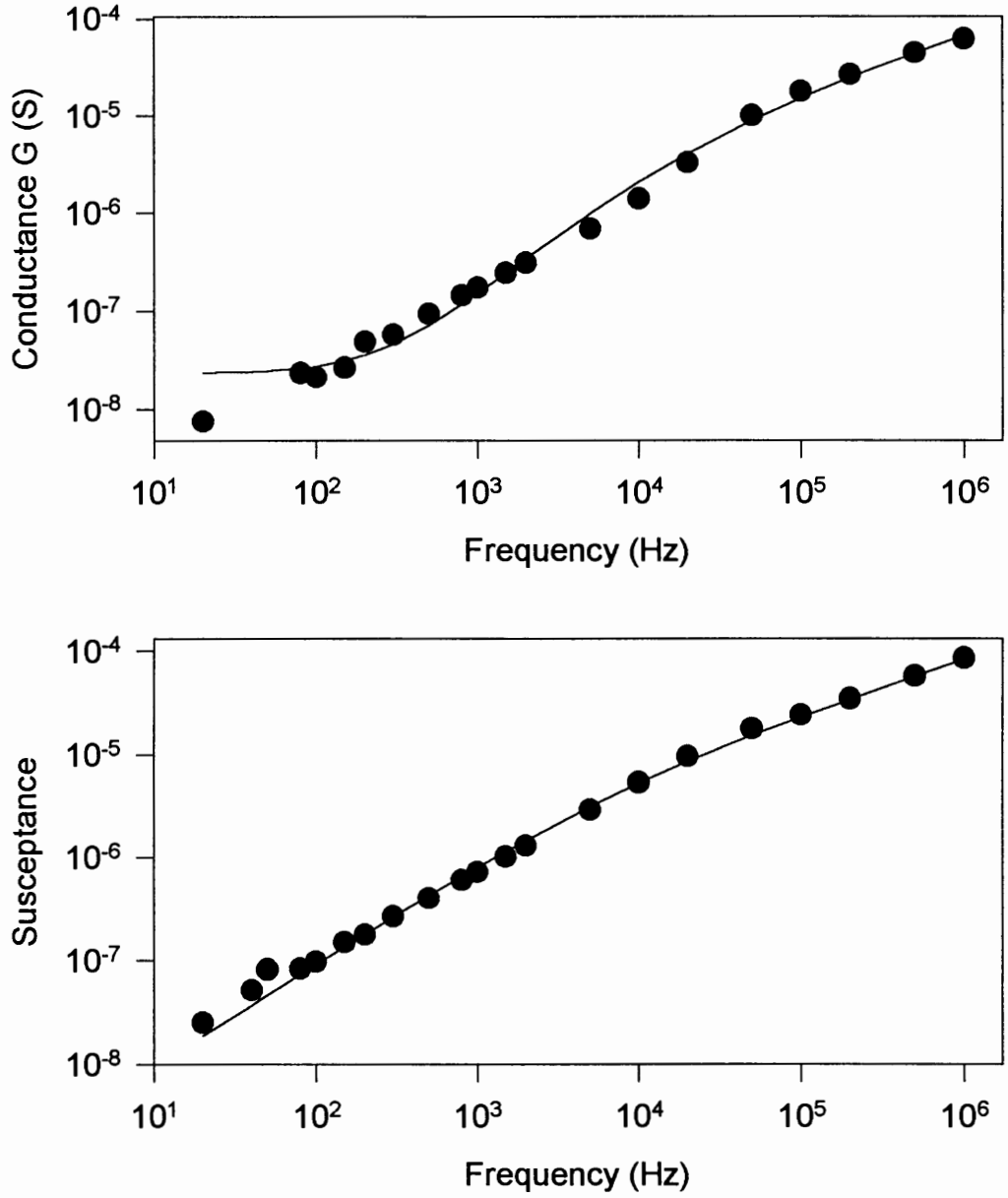

Figure 27: The admittance spectra of a BLM on a teflon insulated silver wire after 96min at 50mV The circuit shown in Figure 23 was used for fitting. A self-inductance of 0.24 μH, resulting from the cables and a stray capacitance of 5pF, was determined.

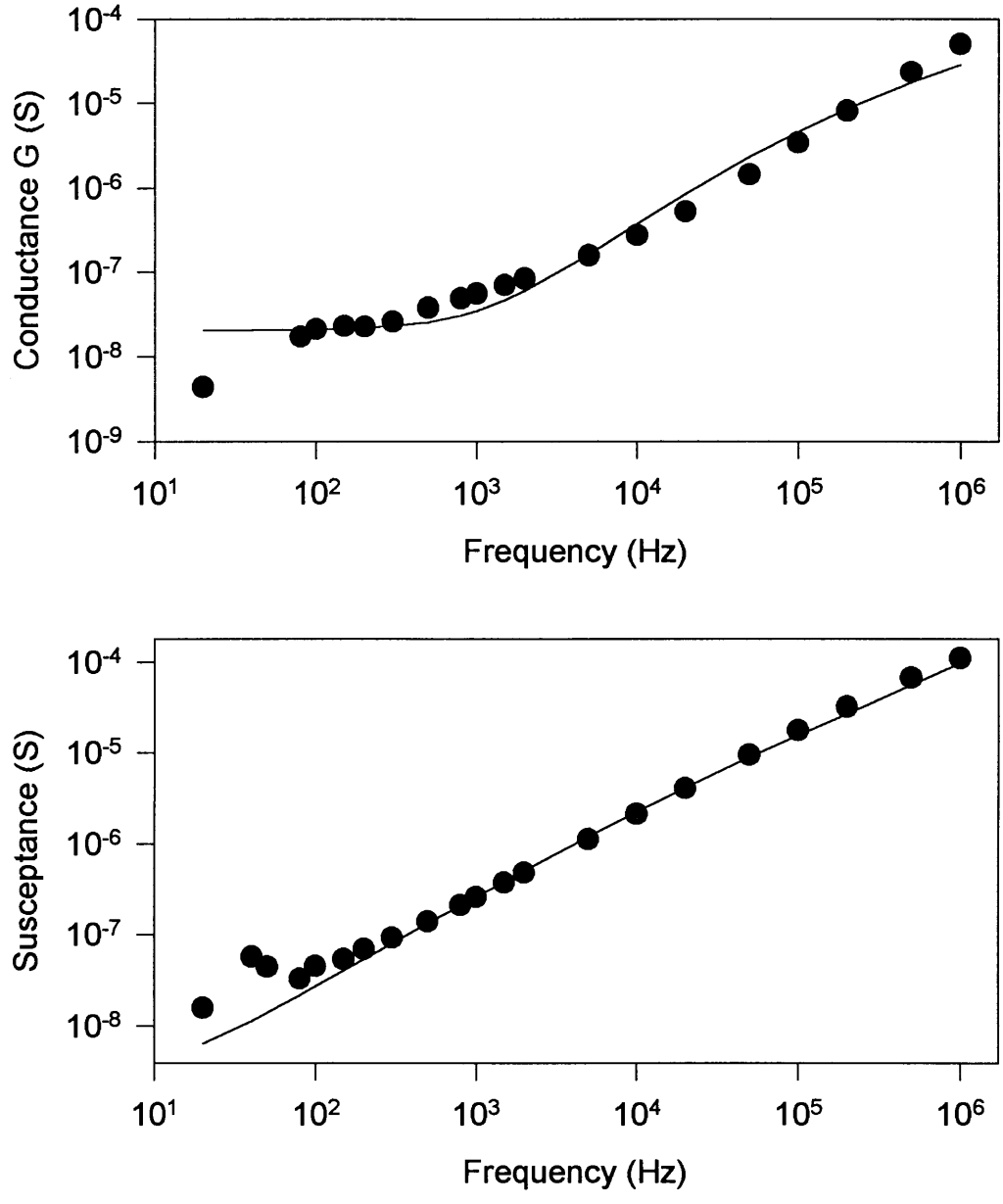

Figure 28: The admittance spectra of a BLM on a teflon insulated steel wire after 86min at 50mV. The circuit shown in Figure 23 was used for fitting. A self-inductance of $0.24\mu H$, resulting from the cables and a stray capacitance of 10pF, was determined.

General features of elements of equivalent circuit for wires with lipid membrane

To obtain a good fit to the experimental spectra it was necessary to account for the equivalent stray and inter-electrode capacitance represented by the capacitor C_2. The values of C_2 employed in fitting the data were C_2=10 pF, for the steel wire, and C_2 = 5 pF for the silver wire. Both values are within the capacitance ranges measured earlier and shown in Figure 22. The presence of self-inductance L_1, accounting for the self inductance of cables, in the circuit had no impact on the fit. However, the value of $L_1 = 0.24$ μH was included in the circuit for completeness since it was found essential in earlier studies.

The physical assignment of circuit elements C_1, R_1 and σ is as follows: C_1 represents the membrane capacitance in series with that of the double layer, R_1 is the charge transfer resistance for the membrane in series with the metal/membrane interface, and the Warburg-type impedance σ accounts for the combination of diffusion limitation, roughness of the surface and defects in the lipid membrane.

Capacitance C_1 The assignment of C_1 to the capacitance of lipid bilayer membrane is based on several experimental results.

- First, it was possible to follow the thinning of lipid film on the cut teflon insulated silver wire (data shown in Figure 29).

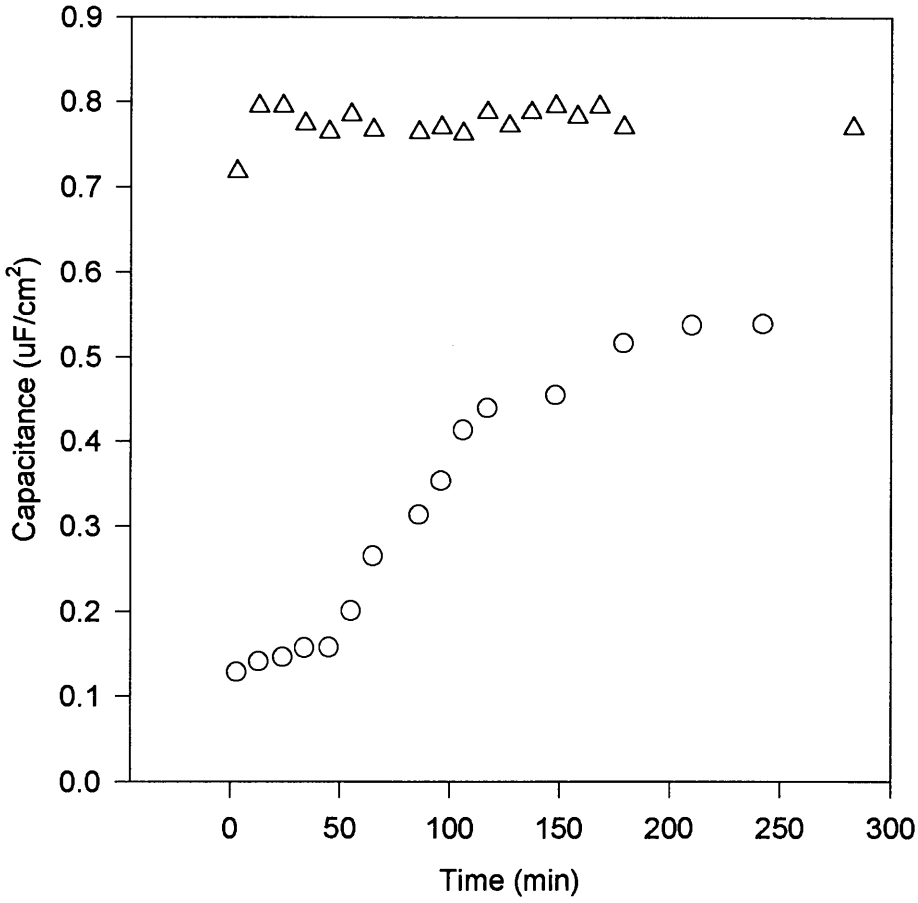

Figure 29: The time dependence of the capacitance of a BLM on a teflon insulated silver (◯) and steel (△) wire immersed in 0.1M KCl solution. On the silver wire a thinning process is observed.

- Second, the value of C_1 normalized to cross sectional area of the wire is comparable to the specific capacitance of the lipid bilayer which is about 0.5 $\frac{\mu F}{cm^2}$. As the data in Table 8 indicate, the capacitance C_1 increased from 0.1 $\frac{\mu F}{cm^2}$, measured 3 minutes after the immersion into KCl solution, to 0.5 $\frac{\mu F}{cm^2}$ after three hours. The thinning process is well known for unsupported lipid bilayer membrane. Membranes formed on steel wire formed more rapidly. The time dependence of capacitance C_1 for silver and steel wires are shown in Figure 29.

- Third, the studies of voltage dependence of admittance spectra showed that the capacitance C_1 increased with the applied voltage. This effect has also been observed for unsupported lipid bilayers and is associated with electrostriction, the effect of compression of lipid bilayer resulting in membrane thinning. Data illustrating the effect of applied voltage on capacitance C_1 are given in Table 9 for membranes formed on the silver wire and in Table 11 for the steel wire.

Resistance R_1 The resistance R_1 is associated with the charge transfer across the membrane and across the metal/membrane interface. The value of this resistance was on the order of 10^7 Ω. It was found that within the experimental error, the value of resistance R_1 was independent of time and independent of voltage (Tables 8 - 11). The value of R_1 normalized to wire cross sectional area was found to be

10^3 Ωcm^2 for the steel wire and $10^4 \Omega cm^2$ for the silver wire. Since the silver surface was found to corrode in our studies with bare cut wires, we assume that the greater value of R_1 of the silver wire is due to the growth of AgCl below the inner membrane surface surface. Thus in the case of silver wire there is an additional resistance in series with the resistance of lipid bilayer.

We found that the normalized resistance R_1 is several orders of magnitude smaller than the resistance of the unsupported lipid bilayer membrane. Similar observation was noted by Tien [WT90]. The origin of the greater conductivity of self-assembled lipid bilayers on cut wires is not understood. It is thought that due to the roughness of the cut metallic surface the surface density of defects in the lipid bilayer is responsible for greater transmembrane conductivity [WT90]. The greater transmembrane conductivity is undesirable feature for the use of these membranes as conductivity sensors because it reduces the sensitivity of transduced signals.

Warburg-type impedance σ We have found that the presence of nonlinearity associated with the Warburg-type equivalent circuit element is necessary to reproduce the admittance spectra of cut teflon insulated wires coated with the lipid film. We have analyzed the data in terms of Randles' equivalent circuit (Figure 24) in which the Warburg impedance was included in parallel to the interfacial capacitance

(C_1 in our circuit) and concluded that the admittance spectra can be reproduced better with Warburg-type element in series with the parallel pair R_1 and C_1.

From the observation of time dependence of formation of the lipid bilayer film on the silver wire (see data in Table 8) we conclude that the Warburg-type element is closely related to the process of formation of lipid bilayer at the surface of metal. For the silver wire the time dependent increase of capacitance C_1 was correlated with the decrease of Warburg-type impedance σ. For steel wire the Warburg-type impedance was independent of time as was the capacitance C_1. Furthermore, σ was found to be independent of the applied voltage.

We associate the presence of Warburg-type element with the roughness of the interface at which the charge transfer is taking place. This assignment is supported by the observation that the impedance spectra of lipid bilayers formed on smooth gold surface reported by Plant [PGY94] could be modeled by the classical interface circuit consisting of discrete R and C elements without the need to introduce the Warburg-type impedance. The position of Warburg element in series with the interfacial R_1 C_1 suggest that the diffusion limitation impede the charging and discharging of the interfacial capacitor C_1.

time (min)	R_1 ($k\Omega cm^2$)	C_1 ($\frac{\mu F}{cm^2}$)	σ ($M\Omega s^{-\frac{1}{2}}$)
3	2.86	0.129	42.4
13	11.4	0.141	33.5
24	16.2	0.146	31.1
34	16.1	0.157	28.9
45	14.8	0.158	27.1
55	17.0	0.170	25.3
65	17.4	0.201	22.7
75	25.5	0.265	19.5
86	19.4	0.314	17.1
96	15.4	0.354	15.2
106	12.7	0.414	14.1
117	12.7	0.414	11.4
148	18.9	0.456	9.29
179	12.6	0.517	5.84
210	15.8	0.538	5.57
242	16.0	0.540	5.21

Table 8: The time dependence of a self-assembled bilayer lipid membrane on the tip of a teflon insulated silver wire in a bathing solution containing 0.1M KCl. The values were obtained at 50mV. C_2 (stray capacitance) was found to be constant, 5pF, L_1 (self inductance) 0.24μH and R_2 as 1000Ω.

Voltage (mV)	R_1 ($k\Omega cm^2$)	C_1 ($\frac{\mu F}{cm^2}$)	$\sigma(M\Omega s^{-\frac{1}{2}})$
10	5.744	0.077	22.1
20	2.145	0.126	43.8
50	2.857	0.140	42.4
70	12.03	0.157	32.0
80	12.47	0.164	31.4
100	12.81	0.170	29.3
120	14.29	0.184	27.9

Voltage (mV)	R_1 ($k\Omega cm^2$)	C_1 ($\frac{\mu F}{cm^2}$)	$\sigma(M\Omega s^{-\frac{1}{2}})$
10	15.37	0.137	36.8
20	14.98	0.139	35.4
50	11.39	0.153	33.5
70	14.43	0.164	29.6
80	16.44	0.172	29.4
100	15.46	0.184	28.0
120	15.81	0.198	26.8

Voltage (mV)	R_1 ($k\Omega cm^2$)	C_1 ($\frac{\mu F}{cm^2}$)	$\sigma(M\Omega s^{-\frac{1}{2}})$
10	27.93	0.292	17.1
20	47.42	0.345	18.5
50	19.39	0.340	17.1
70	23.56	0.424	15.4
80	21.55	0.435	15.1
100	22.04	0.460	14.6
120	24.10	0.493	14.1

Voltage (mV)	R_1 ($k\Omega cm^2$)	C_1 ($\frac{\mu F}{cm^2}$)	$\sigma(M\Omega s^{-\frac{1}{2}})$
10	19.00	0.566	5.24
20	15.37	0.577	5.19
50	16.00	0.601	5.20
70	14.58	0.626	5.08
80	15.17	0.650	5.02
100	16.54	0.696	5.02
120	15.81	0.710	4.96

Table 9: The voltage dependence of fitted values for silver wire immediately after immersion in 0.1M KCl, 10, 73, and 242 minutes later. Values for C_2 (stray capacitance) and for L_1 (self inductance of cables) are set to 5pF and $0.24\mu H$

time (min)	R_1 ($k\Omega cm^2$)	C_1 ($\frac{\mu F}{cm^2}$)	σ ($M\Omega s^{-\frac{1}{2}}$)
3	1.127	0.718	33.8
13	1.224	0.795	36.9
24	1.299	0.795	36.9
34	1.303	0.774	33.3
45	1.246	0.765	33.0
55	1.414	0.785	33.6
65	1.577	0.767	32.8
86	1.551	0.765	31.5
96	1.825	0.770	33.3
106	1.471	0.763	30.9
117	2.152	0.788	33.8
127	1.794	0.772	30.5
137	2.107	0.788	32.5
148	1.962	0.795	31.7
158	2.041	0.783	31.9
168	1.962	0.795	31.7
179	1.886	0.770	32.3
283	1.913	0.770	37.1

Table 10: Time dependence of a self-assembled bilayer lipid membrane on the tip of a teflon insulated steel wire in a bathing solution containing 0.1M KCl. The values were obtained at 50mV. C_2 (stray capacitance) was found to be constant at a value of 10pF, L_1 (self inductance) at a value of 0.24μH and R_2 at a value of 1000Ω.

Voltage (mV)	R_1 ($k\Omega cm^2$)	C_1 ($\frac{\mu F}{cm^2}$)	σ ($M\Omega s^{-\frac{1}{2}}$)
10	1.105	0.718	33.8
20	1.043	0.749	37.4
50	1.127	0.788	38.8
70	1.034	0.804	36.2
80	1.060	0.819	36.6
100	1.007	0.847	35.7
120	9.675	0.887	35.8

Voltage (mV)	R_1 ($k\Omega cm^2$)	C_1 ($\frac{\mu F}{cm^2}$)	σ ($M\Omega s^{-\frac{1}{2}}$)
10	1.264	0.790	39.6
20	1.281	0.795	41.2
50	1.299	0.795	36.9
70	1.166	0.792	33.7
80	1.197	0.813	34.4
100	1.100	0.833	34.3
120	1.056	0.865	33.4

Voltage (mV)	R_1 ($k\Omega cm^2$)	C_1 ($\frac{\mu F}{cm^2}$)	σ ($M\Omega s^{-\frac{1}{2}}$)
10	1.409	0.722	32.6
20	1.507	0.738	41.2
50	1.957	0.795	32.3
70	1.895	0.790	31.5
80	1.842	0.801	31.7
100	1.604	0.813	30.6
120	1.555	0.835	30.9

Table 11: Voltage dependence of fitted values for a BLM on the tip of a steel wire immediately after immersion in 0.1M KCl, 20 minutes later and after 153 minutes. Values for C_2 (stray capacitance) and for L_1 (self inductance of cables) are fixed at 10pF and 0.24μH. R_2 was fixed at 1000 Ω.

4.2 Characterization of TiO_2 systems

A bilayer lipid membrane formed on the tip of teflon insulated wire and a solar cell appear to be two totally different systems. However, closer examination reveals that those two systems are quite similar.

The TiO_2 -based solar cell consists of two electrodes separated by a TiO_2 layer and a nonaqueous electrolyte. In comparison, the lipid bilayer built on an electrode immersed in an ionic solution is a structually similar system. In this sense it is not surprising to find that the admittance spectra of the TiO_2-based solar cell can be reproduced with similar equivalent circuits.

We found it necessary to determine the properties of the cell without TiO_2 and subsequently increase the complexity of the cell. In Section 4.2.1 the admittance spectra of the cell without the TiO_2 -layer and ionic solution is discussed. In Section 4.2.2 we describe results for the similar cell with the TiO_2 while the I_2/I_3^- concentration in the cell is increased. Finally, in Section 4.2.3 we compare the admittance spectra of the solar cell in the dark with those for the illuminated solar cell and discuss the changes of the circuit parameters.

4.2.1 Characterization of the cell in absence of TiO_2

We characterized the cell consisting of the conductive glass electrode, which is used as support for the TiO_2 -layer, the spacer and the Pt-electrode (with an area of

Medium	ϵ of medium	C_1 (pF)	exp. $\frac{A}{d}$
air	1	8.7	0.42m
plastic	3	11.7	0.42m
Octanol	10.3	38.5	0.37m
Ethanol	24.3	90.4	0.40m

Table 12: The capacitances of different electrolytes in a simple setup cell at 100 mV. The values for $\frac{A}{d}$ are calculated by subtracting 5pF for the plastic border of the spacer and stray capacitance and dividing by ϵ_r and ϵ_0. Values for the ϵ_r of the electrolytes were adapted from the reference [Wea70]

$1cm^2$). The cell was filled with media consisting of air, organic polymer, octanol, and ethanol. Capacitances of the system were calculated from the susceptance using the relation

$$C = \frac{B}{2\pi f}$$

To determine the value of the capacitance of this system, two corrections had to be made. First, the border of the plastic spacer also introduced a capacitance, which is in parallel to the capacitance of the medium filled capacitor. Second, stray and cable capacitances also contribute to the capacitance. The obtained data for C_1 were fitted to

$$C = C_0 + C_1(\epsilon_r)$$

$$C_1 = \epsilon_0 \epsilon_r \frac{A}{d}$$

The results obtained for C_1 and $\frac{A}{d}$ are shown in Table 12. The average value of $\frac{A}{d}$ is 0.40m. The spacer has an area of 0.75 cm^2 and a thickness of 0.2mm.

I_2/I_3^--concentration	R_2 (Ω)	C_1 (μ F)	C_2 (pF)	L_1	$\sigma(\Omega s^{-\frac{1}{2}})$
0	13000	5.44	120	(10)	22900
0.5mM	1510	3.82	125	(13.2)	14500
5.0mM	471	2.05	269	58.0	4400
50 mM	90.7	3.08	866	60.9	2970
500mM	40.0	10.4	1070	62.5	2780

Table 13: The values of the equivalent circuit dependent on the concentration of the I_2/I_3^- in a solution of 80% Ethylencarbonate and 20% Propylencarbonate at 100mV. The values in brackets are results from the program fit, but are not effecting the fit.

Taking into account for the contribution of the spacer we obtain a theoretical value of $\frac{A}{d} = 0.38m$. C_0 was found to be 5pF.

The conductance was found to be below the sensitivity limit of the LCR-meter, i.e. smaller than 10^{-9} Siemens.

4.2.2 Cell with TiO_2 in presence of I_2/I_3^-

A large change in the properties of the cell was found in the presence of an I_2/I_3^- solution in the cell. We have found that the equivalent circuit shown in Figure 30 can reproduce the admittance properties of the solar cell in the dark as well as under illumination. The resistor R_1 and capacitance C_1 in parallel represent the photoactive interface of TiO_2, the Warburg-type element σ accounts for the diffusion limitation within the porous TiO_2 layer, the series resistor R_2 accounts for the solution resistance and the inductor L_1 accounts for the self inductance in the circuit. The studies of admittance properties for various circuits indicated that it is essential

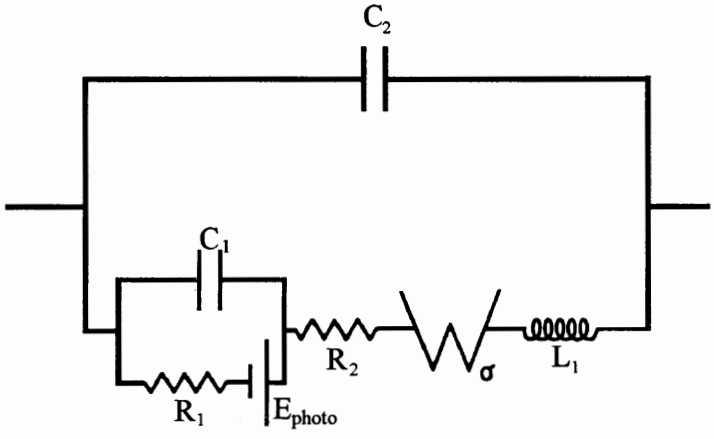

Figure 30: The equivalent circuit used for fitting the data for the TiO_2-based solar cell. The dc-potential E_{photo} was only present in the illuminated solar cell.

for the fit of the experimental spectra, at high frequencies, that capacitance C_2 is in parallel to inductance L_1. The charge separation process operating under illumination and resulting in the generation of dc voltage is represented by the battery E_{photo}.

To identify the circuit elements associated with the presence of I_2/I_3^-, the concentration of I_2/I_3^- was varied. In Table 13 we have summarized the values of individual circuit elements as the concentration of I_2/I_3^- changed. The notable changes are in the value of resistance R_2, the ohmic interelectrode resistance of the of the cell, the cell capacitance C_2 and the Warburg-type impedance σ. First, the value of resistance R_2 decreased from 13kΩ in the absence of I_2/I_3^- to 40Ω for 500mM I_2/I_3^- concentration. The cell capacitance C_2 increased from about 120pF in the

System	R_2 (Ω)	C_1 (μF)	C_2 (nF)	L_1 (μH)	σ ($\Omega s^{-\frac{1}{2}}$)
Cell with 500mM I_2/I_3^-	40.0	3810	1.07	58.7	2780
Colar cell in dark	21.6	10600	1.25	59.0	3030
Illuminated solar cell	18.9	12100	1.61	59.1	3100

Table 14: The values for different setups of the solar cell in presence of 500mM I_2/I_3^- at 100mV.

absence of I_2/I_3^- to 1070pF for 500mM I_2/I_3^- concentration. The origin of this capacitance increase is unknown, it appears as if the dielectric constant of the I_2/I_3^- solution rapidly increased with the increase in I_2/I_3^- concentration. The association of Warburg-type impedance with diffusion limiting processes is supported by the fact that as the concentration of I_2/I_3^- increases, the diffusion limitations are less pronounced as seen by the decrease of the value of Warburg element σ.

4.2.3 Solar cell with porphyrin-sensitized TiO_2 layer in the dark and under illumination

The admittance spectra of the solar cell in the dark are shown in Figure 31. The conductance and susceptance drops in the 100 kHz region and their recovery at higher frequencies are features not seen in the admittance spectra of self-assembled lipid membranes formed on cut wires. This feature requires the presence of L_1 and C_2 elements in the equivalent circuit. The origin of the large value of self-inductance L_1 (59 μH) is unknown. The presence of inductive properties within the solar cell

Voltage		R_2 (Ω)	C_1 (μ F)	C_2 (nF)	L_1 (μ H)	$\sigma(\Omega s^{-\frac{1}{2}})$
10mV	dark	22.2	10.4	1.25	59.0	3040
	light	19.4	12.3	1.61	59.1	3180
20mV	dark	22.0	10.4	1.25	59.0	3040
	light	19.2	12.2	1.61	59.1	3170
50mV	dark	21.8	10.4	1.25	59.0	3050
	light	19.1	12.2	1.61	59.0	3150
70mV	dark	21.7	10.4	1.25	59.0	3040
	light	19.1	12.2	1.61	59.0	3140
80mV	dark	21.6	10.5	1.25	59.0	3040
	light	19.0	12.1	1.61	59.0	3120
100mV	dark	21.6	10.6	1.25	59.0	3030
	light	18.9	12.1	1.61	59.1	3100
120mV	dark	21.5	10.7	1.25	59.0	3030
	light	18.8	12.2	1.61	59.1	3090
1.0V	dark	20.0	95.1	1.49	58.8	3320
	light	17.5	263	1.74	59.0	3300

Table 15: The comparison between the dark and illuminated solar cell at different voltages. The first line of each voltage shows the fitted values for the dark cell, the second line shows them for the illuminated cell.

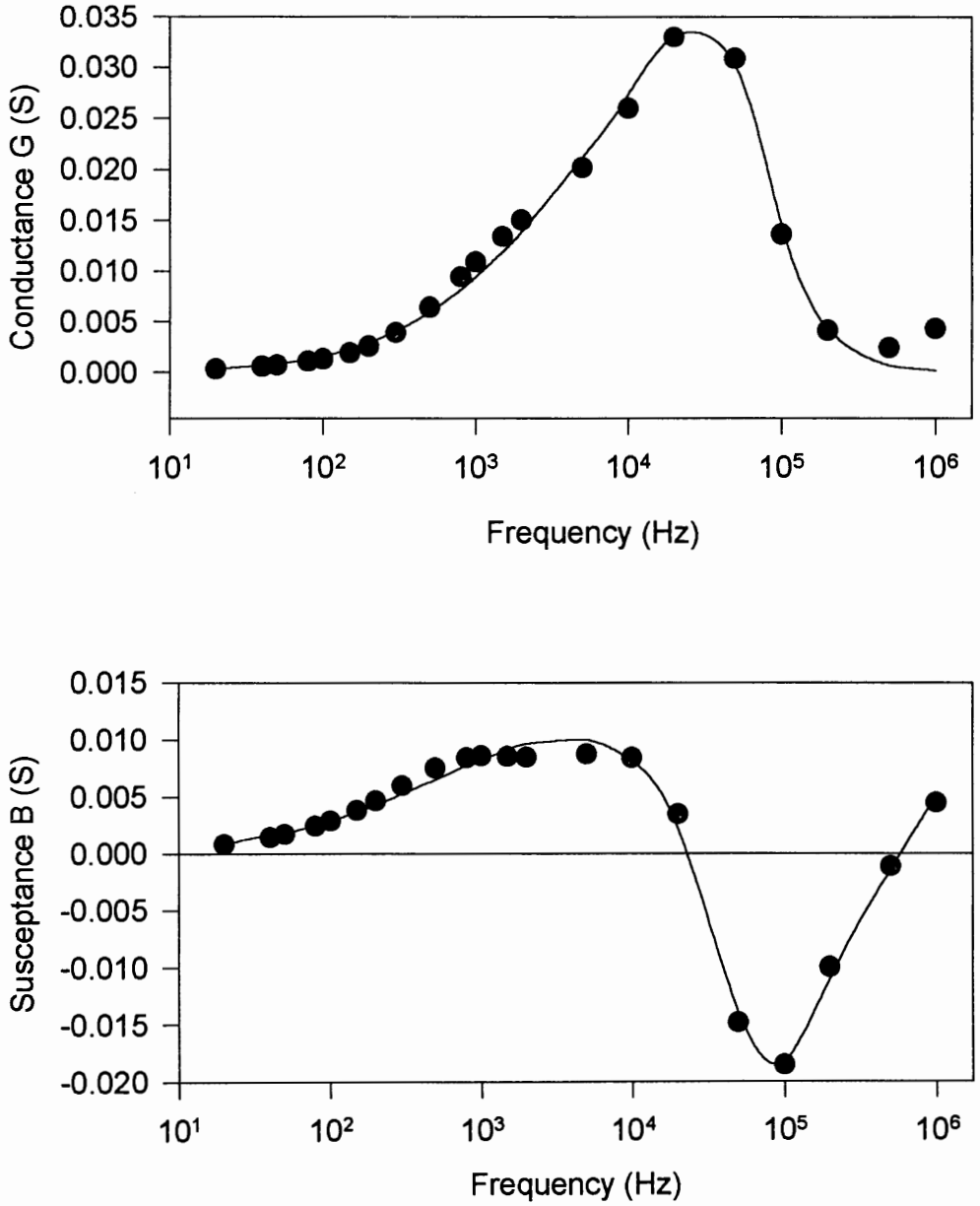

Figure 31: The admittance spectra of the TiO_2-based solar cell in the dark. Spectra were obtained at 100mV.

may due to the adsorption/desorption processes of I_2/I_3^- -pair and I_3^- -ion flux delays within the porous TiO_2 layer. This effect was absent in the lipid bilayer systems where the value of L_1, L_1=0.24 μH, can be understood as self inductance of cables.

The cell was illuminated with a Xenon lamp. The light intensity corresponded to 13 mW/cm^2. Under illumination there were no dramatic changes in the admittance spectra. Although the illuminated cell develops a dc potential difference of 0.42 V and can develop a short circuit current of 51.2 μA, the parameters of the equivalent circuit changed only slightly. In Table 15 we have compared the values of R_2, C_1, C_2 , and σ as a function of amplitude of the ac voltage. There is a distinct switching of values of these parameters associated with the presence of light. On illumination R_2 decreases, C_1 , C_2 and σ increase. The switching is not understood and can be addressed using kinetic models of charge movement within the solar cell.

Chapter 5

Conclusions

We have done studies on properties of elements comprising the measuring cell, individually and in various combinations. These studies included measurements of admittance spectra in the frequency range 20 Hz - 1 MHz of

- Two sintered Ag/AgCl electrodes in KCl solution, since the Ag/AgCl electrode is used as the reference electrode when measuring properties of lipid films.
- An empty measuring cell and the cell filled with KCl solution in which the length of the immersed teflon insulated wire was varied.
- Cut teflon insulated silver and stainless steel wires as supports for self-assembled lipid films.

- Cut teflon insulated silver and stainless steel wires coated with self-assembled lipid film at the tip of the wire.

The admittance spectra were analyzed in terms of equivalent circuits used in impedance studies of similar systems reported in literature. We have searched for the simplest equivalent circuit that can reproduce, with one set of parameters simultaneously, the frequency dependence of the conductance and the susceptance. We have found that the systems consisting of (i) two sintered Ag/AgCl electrodes, (ii) the cut teflon insulated steel wire in combination with the Ag/AgCl electrode, and (iii) the cut teflon steel and silver wires with self-assembled lipid films all contained Warburg-type impedance circuit element. In these systems it was possible to assign the individual R and C elements and the Warburg-type impedance to physical units present in the cell and the measuring circuit. These included the interface between the metallic surface of the cut teflon insulated wire and KCl solution in the absence and presence of the self-assembled lipid bilayer. The resistance of the solution and the connecting cables, the self-inductance of the connecting cables, the stray and interelectrode capacitance were also identified as individual elements in the system circuit. The presence of the Warburg-type impedance was associated with the roughness of the interface at which the charge transfer is taking place.

The major finding of the present work is that the use of simple equivalent RC circuits to represent electrical properties of self-assembled lipid bilayer formed on cut

insulated wires is inadequate. This was made apparent by studying the properties of the impedance spectra over the wide range of frequency.

In addition to self assembled lipid bilayers formed on cut teflon insulated wires we have studied a solar cell based on porphyrin-sensitized porous TiO_2 layers in contact with an I_2/I_3^- redox pair. To construct an equivalent circuit of the cell we have measured the admittance spectra of the cell with an increasing number of components comprising the solar cell. In this manner it was possible to arrive at equivalent circuit that can reproduce the experimental admittance spectra and can be physically associated with the major structures or regions of the solar cell. The photoactive interface, with the adsorbed porphyrin layer at which charge separation under illumination is taking place, can be represented by a capacitor in parallel with resistor in series with light generating electromotive force represented by a battery. The battery represents the photovoltage which charges the interfacial capacitor.

In series with the interface region is the porous TiO_2 which is represented by Warburg-type impedance element necessary to model the diffusion limited transport of the I_2/I_3^- pairs within the pores of the TiO_2 layer. The additional series element is the ohmic resistance that models the space between the TiO_2 layer and the platinum counter electrode. To model the admittance in the 100 kHz - 1 MHz region it was necessary to introduce the self inductance and the cell capacitance. The origin of these is not well understood.

Based on the experience gained in these exploratory studies we recommend

- building instrumentation which would extend the method to a frequency region below 20 Hz, the current limit of the LCR bridge
- setting up a three electrode system that would allow control of the potential bias relative to the potential of the solution
- to continue the work with self-assembled lipid membranes with the emphasis being to increase the internal resistance of the metal/lipid bilayer/electrolyte interface
- to continue the work on the porphyrin-sensitized TiO_2 solar cell in order to understand not only the anomalous self inductance, but build a model based on the structural, kinetic and thermodynamic properties of the TiO_2 layer.

Bibliography

[AR71] R. D. Armstrong and W. P. Race. Double layer capacitance dispersion at the metal-electrolyte interface in the case of a dilute electrolyte. *Electroanalytical Chemistry and Interfacial Electrochemistry*, 33:285–290, 1971.

[BCY80] John O'M. Bockris, Brian E. Conway, and Ernest Yeager. Comprehensive treatise of electrochemistry. In *Volume1: The Double Layer.* Plenum Press, New York, 1980.

[Ber96] P. Bergveld. The future of biosensors. *Sensors and Actuators*, A56:65–73, 1996.

[BR70] John O'M. Bockris and Amulya K. N. Reddy. *Modern Electrochemistry 1,2.* Plenum Press, New York, 1970.

[CK92] Hans G.L. Coster and K.J. Kim. Characterisation of ultrafiltration membranes by impedance spectroscopy. *Journal of Membrane Science*, 66:19–26, 1992.

[Col68] Kenneth S. Cole. *Membranes, Ions and Impulses.* University of California Press, Berkeley, 1968.

[CS74] Hans G.L. Coster and J.R. Smith. The molecular organisation of bimolecular lipid membranes. *Biochimica et Biophysica Acta*, 373:151–164, 1974.

[DA75] Farrington Daniels and Robert A. Alberty. *Physical Chemistry.* John Wiley & Sons, Inc, New York, London, Sydney, Toronto, 1975.

[dL67] Robert de Levie. Electrochemical response of porous and rough electrodes. *Advances in Electrochemistry and Electrochemical Engineering*, 6:329–397, 1967.

[dL90] Robert de Levie. Fractals and rough electrodes. *Journal of Electroanalytical Chemistry*, 281:1–21, 1990.

[dLTA75] Robert de Levie, John W. Thomas, and Kathleen M. Abbey. Membrane admittance measurements under computer control. *Electroanalytical Chemistry and Interfacial Electrochemistry*, 62:111–125, 1975.

[dLV90] Robert de Levie and Andrew Vogt. On the electrochemical response of rough electrodes. part ii. the transient response in the presence of slow

faradaic processes. *Journal of Electroanalytical Chemistry*, 281:23–28, 1990.

[DS95] E. A. Dislavo and S. A. Simon. *Permeability and stability of lipid bilayers.* CRC Press, Boca Raton, 1995.

[EJ90] W. Eberling and Jean-Claude Justice. Frequency dependent conductance and dielectric permitivity. *Journal of Solution Chemistry*, 19(9):945–955, 1990.

[Far90] Thomas L. Fare. Electrical characterization of dipalmitoylphospha tidylethanolamine and cadmium stereate films on platinum surfaces in aqueous solutions. *Langmuir*, 6:1172–1179, 1990.

[Göp96] Wolfgang Göpel. Ultimate limits in the miniaturization of chemical sensors. *Sensors and Actuators A*, 56:83–102, 1996.

[Gra57] F. A. Grant. Use of complex conductivity in the representation of dielectric phenomena. *Journal of Applied Physics*, 29(1):76–80, January 1957.

[H+92] A. Hagfeldt et al. Photoelectrochemical studies of colloidal TiO_2 films: the charge separation process studied by means of action spectra in the UV region. *Solar Energy Materials and Solar Cells*, 27:293–304, 1992.

[Hal75] James. E. Hall. Access Resistance of a Small Circular Pore. *The Journal of general Physiology*, 66, 1975.

[Hon94] Felix T. Hong. Electrochemical processes in membranes that contain bacteriorhodopsin. In Martin Blank and Igor Vodyanoy, editors, *Biomembrane electrochemistry*, pages 531–560. American Chemical Society, 1994.

[JI69] G.J. Janz and D. J. G. Ives. Silver, silver chloride electrodes. *Annals New York Academy of Sciences*, 1(1):210–221, 1969.

[Jüt90] K. Jüttner. Electrochemical impedance spectroscopy (eis) of corrosion processes on inhomogeneous surfaces. *Electrochimica Acta*, 35(10), 1990.

[Läu76] P. Läuger. Diffusion-limited ion flow through pores. *Biochimica et Biophysica Acta*, 455:493–509, 1976.

[M+95] R. Murgasova et al. Cyclic coltammetry of supported blms. In A.P. Jardine, editor, *SPIE's 1995 North American Conference on Smart Structures and Materials*, volume 2441, page 33, 1995.

[Mac87] J. Ross Macdonald. *Impedance Spectroscopy.* John Wiley & Sons, New York, 1987.

[Mac90a] Digby D. Macdonald. Review of mechanistic analysis by electrochemical impedance spectroscopy. *Electrochimica Acta*, 35(10):1509–1525, 1990.

[Mac90b] James Ross MacDonald. Impedance spectroscopy: old problems and new developments. *Electrochimica Acta*, 35(10):1483–1492, 1990.

[McA96] E. T. McAdams. Problems in equivalent circuit modelling of the electrical properties of biological tissues. *Bioelectrochemistry and Bioenergetics*, 40:147–152, 1996.

[MCG91] Cary Miller, Pierre Cuendet, and Michael Grätzel. Adsorbed ω-hydrocy thiol monolayers on gold electrodes: Evidence for electron tunneling to redox species in solution. *J. Phys. Chem.*, 95:877–888, 1991.

[MT91] T. Martynski and H. T. Tien. Spontaneous assembly of bilayer membranes on a solid surface. *Bioelectrochemistry and Bioenergetics*, 25:317–324, 1991.

[N+93] M. K. Nazeeruddin et al. Conversion of Light to Electricity by *cis*-X_2Bis(2,2' -bipyridyl-4,4'-dicarboxylate)ruthenium(II) Charge Transfer Sensitizers (X = Cl^-, Br^-, I^-, CN^-, and SCN^-) on Nanocrystalline TiO_2 Electrodes. *J. Ann. Chem. Soc.*, 115:6382–6390, 1993.

[Neu95] Michael R. Neumann. Biopotential electrodes. In J. D. Bronzino, editor, *The biomedical engineering textbook*, chapter 48. CRC Press, Boca, Radon, FL, 1995.

[OL+94] A. Ottova-Leitmannova et al. Self-assembling bilayer lipid membranes on solid support. *Advances in chemistry series*, 240:439–454, 1994. Molecular and biomolecular electronics 1991.

[OT97] A. Ottova and V. Tvarozek. Self-assembled blms: biomembrane models and biosensor applications. *Supramolecular Science*, 4:101–112, 1997.

[PGY94] A.L. Plant, M. Gueguetchkeri, and W. Yap. Supported phospholipid/alkanethiol biomimetic membranes: Insulating properties. *Biophysical Journal*, 67:1126–1133, September 1994.

[Rai90] I. D. Raistrick. Impedance studies of porous electrodes. *Electrochimica Acta*, 35(10):1579–1586, 1990.

[RBBH93] J. Ramos-Barrado, J. Benavente, and A. Herida. Electrical conductivity of different traeted isolated cuticular membranes by impedance spectroscopy. *Journal of Biochemistry and Biophysics*, 346(2):337–341, 1993.

[S+96] C. Steinem et al. Impedane analysis of supported lipid bilayer membranes: a scrutiny of different preparation techniques. *Biochimica et Biophysica Acta*, 1279:169–180, 1996.

[Sch67] H. P. Schwan. Electrode polarization impedance and measurements in biological tissues. *New York Academy of Sciences*, 1:191–209, 1967.

[Sme95] Pavel Smejtek. Permeability of lipophilic ions across lipid bilayers. In E.A. Disalvo and S.A. Simon, editors, *Permeability and Stability of Lipid Bilayers*, chapter 10. CRC Press, Boca Raton, FL, 1995.

[Smy50] W. R. Smythe. *Static and Dynamic Electricity.* McGraw-Hill Book Company Inc, New York, 1950.

[SRS70] M. Sluyters-Rehbach and J.H. Sluyters. Sine wave methods in the study of electrode process. In *Electroanalytical chemistry*, volume 4, pages 1–128. Bard, 1970.

[SS89] M. Stelzle and E. Sackmann. Sensitive detection of protein adsorption to supported lipid bilayers by frequency-dependent capacitance measurements and microelectrophoresis. *Biochimica et Biophysica Acta*, 981:135–142, 1989.

[Sto90] Z. Stoynov. Impedance modelling and data processing: structural and parametrical estimation. *Biochimica Acta*, 35(10):1493–1499, 1990.

[Str88] Lubert Stryer. *Biochemistry.* W.H.Freeman, New York, 1988.

[Tie74] H.T. Tien. *Bilayer Lipid Membranes (BLM): Theory and Practice.* Marcel Dekker, New York, 1974.

[War99] E. Warburg. Über das Verhalten sogenannter unpolarisierbarer Elektroden gegen Wechselstrom. *Ann. Phys. Chem.*, 67:493–499, 1899.

[WBCY80] Ralph E. White, John O'M. Bockris, Brian E. Conway, and Ernest Yeager. Comprehensive treatise of electrochemistry. In *Volume8: Experimental Methods in Electrochemistry.* Plenum Press, New York, 1980.

[Wea70] Robert C. Weast, editor. *Handbook of chemistry and physics.* The chemical rubber Co., 18901 Cranwood Parkway, Cleveland, Ohio, 44128, 1970.

[WT90] A. Wardak and H.T. Tien. Cyclic voltammetry studies of bilayer lipid membranes deposited on platinum by self assembly. *Biochemistry and Bioenergetics*, 24:1–11, 1990.